Chemical Engineering Research and Design 222 (2025) 425–440

Contents lists available at ScienceDirect

Chemical Engineering Research and Design

journal homepage: www.elsevier.com/locate/cherd

An integrated centrifugal microfluidic chip for *in situ* chemical oxygen demand by improving the conventional dichromate method

Z. Wu [a,b,c,1], B.V.N. Sewwandi [a,1], H.M.S.N. Deegala [a], K.M.N.K.B. Kuruppu [a], E.G.V.P. Chandrasekara [a], S.P. Hemachandra [a], L. Pan [c], W. Yang [c], Z. Zhang [c], X. Chen [a,d], A.C.A. Jayasundara [e,2], Rohan Weerasooriya [a,d,*]

[a] *Centre for Water Quality Research, National Institute of Fundamental Studies, Kandy, Sri Lanka, China and Sri Lanka Joint Research and Demonstration Centre for Water Technology, Ministry of Water Supply, Sri Lanka*
[b] *Postgraduate Institute of Science, University of Peradeniya, Peradeniya, Sri Lanka*
[c] *Wuhan New fiber Optics Electron Co., Ltd, Wuhan 430074, PR China*
[d] *Key Lab of Aerospace Structural Parts Forming Technology and Equipment of Anhui Province, Institute of Industry and Equipment Technology, Hefei University of Technology, Hefei 230009, PR China*
[e] *Department of Chemistry, University of Peradeniya, Sri Lanka*

ARTICLE INFO

Keywords:
Centrifugal microfluidic chips
Angular acceleration
Chemical oxygen demand
Euler force
Filtering

ABSTRACT

This study proposed automated centrifugal microfluidic chips (CMCs) as advanced Lab-on-a-Chip systems for water quality analysis, taking chemical oxygen demand (COD) as an example. The CMCs minimize reagent use, reduce hazardous waste, and enable precise reaction control through optimized geometric designs by leveraging centrifugal and Euler forces to enhance particle filtration, liquid transfer, and in situ monitoring. Our novel settling chamber isolated large particles in digested samples, improving the efficiency of COD detection. Simulations were conducted to optimize the inclination angle and angular acceleration of the siphon valve, ensuring stable liquid transfer. The system achieved a 6.85 % improvement in COD detection accuracy, an 88 % reduction in sample volume, and a 55 % decrease in analysis time. Precision increased by 64.10 %, and uncertainty was reduced by 47.04 %, maintaining a detection range of 0–150 mgL^{-1} with a Limit of Detection of 4 mgL^{-1} and a Limit of Quantification of 12 mgL^{-1}. With a compact, portable design (250 mm × 280 mm × 315 mm, 13 kg) and low power consumption (33.9 W), the device is well-suited for environmental monitoring and remote water quality testing. To ensure coherence with the novel CMC chip, we developed the customized CMC microfluidic equipment in our laboratory. Its adaptability for other difficult water quality parameters, such as total nitrogen or phosphorus, could boost its applications in public health and sustainable water management.

1. Introduction

Chemical Oxygen Demand (COD), a key parameter in water and wastewater treatment, represents the total amount of oxygen required to oxidize organic matter in a sample using a chemical oxidant. The regulatory method of COD measurement requires dichromate digestion of organic matter in the sample, followed by a titrimetric or colorimetric detection (ISO, 6060, 1989; ISO15705, 2002). This method is precise and widely used in the water sector; however, it is not suitable for field measurements or automation that often requires measuring large batches of samples (Kumar et al., 2024). Further, to ensure its sustainability and efficiency, this procedure requires minimizing chemical usage and digestion time. Table 1 summarizes an ensemble of dichromate-based COD digestion methods. An overview of COD

* Corresponding author at: Centre for Water Quality Research, National Institute of Fundamental Studies, Kandy, Sri Lanka, China and Sri Lanka Joint Research and Demonstration Centre for Water Technology, Ministry of Water Supply, Sri Lanka.
E-mail addresses: wuzhi@chinhangroup.com (Z. Wu), niluka.be@nifs.ac.lk (B.V.N. Sewwandi), shashini.de@nifs.ac.lk (H.M.S.N. Deegala), nayana.ku@nifs.ac.lk (K.M.N.K.B. Kuruppu), vishva.ch@nifs.ac.lk (E.G.V.P. Chandrasekara), samadhi.he@nifs.ac.lk (S.P. Hemachandra), panling@newfiber.com.cn (L. Pan), yangweiguang@newfiber.com.cn (W. Yang), zhangzhenyang@newfiber.com.cn (Z. Zhang), xingchen@hfut.edu.cn (X. Chen), Jayasunderac@moval.edu (A.C.A. Jayasundara), rohan.we@nifs.ac.lk (R. Weerasooriya).
[1] Shared fist authorship
[2] Present address: (ACAJ) School of Science, Missouri Valley College, MO 65340, USA.

https://doi.org/10.1016/j.cherd.2025.09.019
Received 7 April 2025; Received in revised form 9 August 2025; Accepted 11 September 2025
Available online 12 September 2025

determination methods based on dichromate and non-dichromate oxidation, utilizing various detection principles such as titrimetric, colorimetric, and electrochemical techniques, is also given in Table 1S (Table 1S; Table 1 support documentation). Based on their operational principles, the most effective conventional method in each category, evaluated using key performance indicators such as volume of sample, limit of detection (LOD), limit of quantification (LOQ), precision, accuracy, and Linear Dynamic Range (LDR) of detection, is summarized in Table 1S. Despite their widespread use, all conventional COD methods share the following limitations: a. labor-intensive procedures, b. prolonged digestion times (typically around 2–3 h), c. high chemical consumption, d. the need for filtration before detection, e. large analyte uncertainty, f. limited portability and automation, and g. excessive waste generation (Huang and Jiang, 2025; De Vito-Francesco et al., 2022).

On the other hand, "Lab-on-a-Chip" (LOC) devices, including lab-on-a-compact disc (LOCD) and centrifugal microfluidic chips (CMCs) have demonstrated significant potential to improve the efficiency of water quality analysis (Pol et al., 2017). LOCD technology integrates microchannels, reservoirs, and other microfluidic components into a compact disc platform, enabling advanced fluid manipulation and analysis. CMCs are widely used in various biomedical applications, such as nucleic acid analysis, blood sample processing, immunoassays, and point-of-care diagnostics (Farahinia et al., 2023; Guo et al., 2023). However, their application in the water sector remains limited. For instance, Hwang et al. developed a CMC-based system for determining nitrite, nitrate, ammonium, orthophosphate, and silicate in water samples (Hwang et al., 2013), while Lin et al. proposed a microfluidic chip-based sensor for in-situ detection of biochemical oxygen demand (BOD) (Lin et al., 2024). Bhuiyan et al. developed a simple microfluidic chip and a novel automated droplet-based analyzer for in situ monitoring of NH_4^+ concentrations in river water (Bhuiyan et al., 2025). Several non-dichromate oxidation COD measuring techniques suited for in situ COD measurements have also developed using microfluidic technology (Yin et al., 2021; Dong et al., 2024; Xie et al., 2024; Li et al., 2022a; Jiang et al., 2020). Hither to date, most them require specialized sensors and cost intensive (Dong et al., 2024; Xie et al., 2024; Li et al., 2022a; Jiang et al., 2020). Further before using them routinely in water industry, careful data scrutiny is required against regulatory COD measurands' to minimize inconsistency in results. To address many of the aforementioned limitations in conventional COD detection, we developed a CMC-assisted microfluidic method for determining COD in water and wastewater using dichromate digestion enabling compatibility with the regulatory methods (ISO, 6060, 1989; ISO15705, 2002). Further our method significantly reduces chemical and sample consumption while improving user-friendliness, automation, and portability for field-based COD measurements. This technology is particularly well-suited for deployment in remote or resource-limited settings, enabling on-site analysis of COD, BOD, total nitrogen (TN), and total phosphorus (TP) in water and wastewater. Additionally, the CMC cell–integrated microfluidic device can easily be adapted for the determination of total nitrogen and total phosphorus in both water and wastewater samples.

Table 1
Comparison of dichromate oxidation chemical oxygen demand (COD) measurement methods.

Method Name	LDR / mgL^{-1}	LOD/ mgL^{-1}	LOQ mgL^{-1}	Accuracy (%) / RSD (%)	Solution volume / mL	Analysis Time/ min	Temperature/ °C	Notes	Ref
Standard Method									
Open Reflux & FAS Titration	30–700	30	NA	Accuracy< 5	~10	120–180	150	Disadvantage: Toxic chemicals (Cr, Hg); Cl^- interference; expensive chemicals (Ag^+)	(Li et al., 2018; Ma, 2017; Qu et al., 2011)
Closed Reflux & Spectrophotometric	6–1000	6	NA	NA	~2	120	150	Disadvantage: Toxic chemicals (Cr, Hg);	(Li et al., 2018; Ma, 2017)
Closed Reflux & Spectrophotometric _ reduce volume	30–600	3.6	NA	Accuracy1.5	1.5	> 40	150	bubbles, turbidity, and Cl^- interfere	(Carbajal-Palacios et al., 2014)
Modified standard Methods									
Microwave-Assisted $K_2Cr_2O_7$ Digestion& Titration	NA	NA	NA	NA	NA	1–15	170	Disadvantage: Toxic reagents; safety risks; high cost; energy-consuming	(Li et al., 2018; Ma, 2017)
Ultrasound-Assisted $K_2Cr_2O_7$ digestion & titration	NA	NA	NA	NA	NA	> 15	NA	Advantage: Low cost, rapid Disadvantage: Toxic reagents, energy-consuming	(Li et al., 2018)
Chemiluminescence (CL) $K_2Cr_2O_7$ digestion, luminol-H_2O_2 for detection	4–400	2	NA	NA	NA	1.5	RT	Advantage: High sensitivity, low reagent use, fast Disadvantage: toxic reagent consumption	(Li et al., 2018)
HJ/T399–2007 (China)-$K_2Cr_2O_7$ closed reflux Spectrophotometry	NA	NA	NA	NA	NA	60	165	Advantage: Fast, low reagent use Disadvantage: Narrow linear range	(Ma, 2017)
Electromagnetic Induction Heating -$K_2Cr_2O_7$ -Titration (FAS)	NA	NA	NA	NA	NA	8	145	NA	(Ma, 2017)
New Techniques									
Smartphone-based Colorimetry Potassium dichromate digestion	0–150	NA	NA	Accuracy. 97	2	> 120	150	Advantages: Low-cost, portable, decentralized Disadvantages: Image quality dependency, chlorine interference, linear interpolation errors	(de Castro et al., 2023)

NA: not available; RT: room temperature.

Active microfluidic separation uses external forces (electric, magnetic, or centrifugal) for precise particle control, but complex chip designs limit environmental applications. Zhao et al. developed a centrifugal microfluidic chip (iExoDisc) for automated plasma exosome isolation, though membrane integration can lead to sealing issues, clogging, and reduced performance (O'Connell and Landers, 2023). Hwang et al. employed centrifugal forces with a sawtooth design to separate particulates in water (Hwang et al., 2013). Feng et al. used a multi-stage CMC to size-selectively isolate microplastics (MPs) smaller than 63 μm, specifically designing the system for multi-stage sorting and detection based on particle size at the micron scale; however, they did not analyze or focus on the separated fine solid-free solution (Feng et al., 2025).

Therefore, we employed centrifugal microfluidic chip technology for the in-situ detection of COD in water. The microfluidic equipment available in the market does not accommodate the cell platform we fabricated specifically for the COD detection. Therefore, the entire microfluidic equipment was fabricated in our laboratory to ensure coherence with the novel CMC platform and subsequent automation in the field. The CMC platform utilizes centrifugal, Coriolis, and Euler forces generated by chip rotation to provide precise fluid control with simple, motor-driven operation. Thus, optimizing the geometry of the microfluidic chip is essential for achieving efficient flow regulation, accurate analyte detection, and reproducible results. Notably, passive siphon valves require only a rotating motor for actuation, eliminating the need for external components or manual intervention (Deng et al., 2014a; Lu et al., 2024a). These valves operate by modulating the chip's motion to facilitate fluid pumping. They also enhance solution homogeneity, enable sequential fluid transfer and mixing, and significantly reduce processing time.

To maximize their functionality, CMC designs can be tailored and optimized through iterative experimental and computational fluid dynamics (CFD) simulations (Cai et al., 2023; Lu et al., 2024b). These simulations help fine-tune geometrical parameters such as chamber depth, channel width, siphon dimensions, and rotation profiles to achieve optimal flow control, minimal dead volume, and enhanced particulate separation (Lu et al., 2024a). Such optimization is particularly crucial when dealing with real environmental samples that contain colloids or precipitates, which may otherwise compromise detection accuracy. The fabricated CMC platform was not compatible with standard commercial microfluidic equipment; therefore, we designed dedicated microfluidic equipment to meet current stringent performance requirements.

We have developed a microfluidic method for COD detection with the following objectives: (i) to design a cell platform incorporating a membrane-free particulate filtration mechanism; (ii) to optimize fluid transfer efficiency within the CMC cell assembly by computationally adjusting Euler centrifugal forces, thereby enhancing sequential liquid release and siphon valve discharge; and (iii) to develop dedicated microfluidic equipment integrating a high-throughput CMC platform, enabling automation capabilities. This microfluidic COD detection method significantly improves the sensitivity, accuracy, and robustness of analytical measurements. Further, this method significantly reduces chemical and sample consumption while improving user-friendliness, automation, and portability for field-based COD measurements. This technology is particularly well-suited for deployment in remote or resource-limited settings, enabling on-site analysis of COD, BOD, total nitrogen (TN), and total phosphorus (TP) in water and wastewater. Additionally, the CMC cell–integrated microfluidic device can easily be adapted for the determination of total nitrogen and total phosphorus in both water and wastewater samples.

2. Materials and methods

2.1. Materials

2.1.1. Reagents

A standard solution of potassium hydrogen phthalate (KPH), and certified 5000 mgL^{-1} KPH standards were purchased from Tanmo Quality Inspection- Standard Material Centre (TMRM) (ID: BW20004–5000–500, CAS: 14431–43–7). Analytical grade sulfuric acid (H_2SO_4) with 98 % purity, silver sulfate (Ag_2SO_4) with $\geq$ 98.5 % purity and mercury sulfate ($HgSO_4$ with $\geq$99.7 % purity, and pharmaceutical grade potassium dichromate ($K_2Cr_2O_7$) with $\geq$ 99.95 % purity was purchased from Sinopharm Group Chemical Reagent Co., LTD (China).

2.1.2. Cell materials

The three-dimensional (3D) model of the centrifugal microfluidic chip was designed using AutoCAD software. Polymethyl methacrylate (PMMA) was used to fabricate the chip's injection-molded components, while quartz glass was incorporated with PMMA for the upper and lower detection sheets (Shenzhen Xintao New Materials Co., Ltd, China). Polyethylene Terephthalate (PET) was chosen for the preparation of the upper and lower double-sided adhesive tape and pressure-sensitive adhesive (PSA) due to its excellent thermal and dimensional stability (Nanofilm Materials Co., Ltd, China).

2.2. Methods

2.2.1. Microfluidic cell and equipment development

We developed a new CMC cell along with dedicated microfluidic equipment tailored for COD detection. The following sections, together with the accompanying supporting documents, outline the fabrication details of both the cell and the equipment (Fig. 1, Fig. 2 and Section 2S).

2.2.1.1. Fabrication of centrifugal microfluidic chips. First, the filtered water sample is injected into the equipment port (Figure S1), where it is carried over to the loading / in situ digestion chamber (Fig. 1A & Fig. 1B). The digestion process produces solid residues, including inorganic precipitates such as metal oxides and hydroxides, as well as non-digestible solids and salts formed during reagent reactions. These residual particles scatter light and interfere with optical measurements, making effective residue management critical for maintaining analytical precision and avoiding contamination. To address this, the chip integrates three pre-waste pools to the left and above the quantitative chamber (Fig. 1A). These strategically placed pools are designed to trap residual solids before the sample advances to subsequent processing zones (Fig. 1C). At the center of the chip lies the digestion sample quantitative pool, which ensures accurate and consistent sample volume for downstream reactions (Fig. 1A). To manage excess reagents and prevent backflow, a post-waste pool is placed to the left of the quantitative chamber. This chamber collects overflow liquids and contributes to unidirectional flow control, minimizing the risk of cross-contamination (Fig. 1A).

Fluid transfer from the quantitative area to the detection pool is precisely controlled by a siphon valve system located at the bottom of the quantitative chambers (Fig. 1A). The flow is further regulated by a throttling valve, which consists of long and narrow microchannels that introduce hydraulic resistance. This throttling mechanism allows a slow and controlled passage of liquids, ensuring proper reaction timing and enhancing mixing efficiency (Fig. 1C). The reagents are released and mixed with the digested sample to initiate the colorimetric reaction required for COD or other target analyte detection. The final step occurs

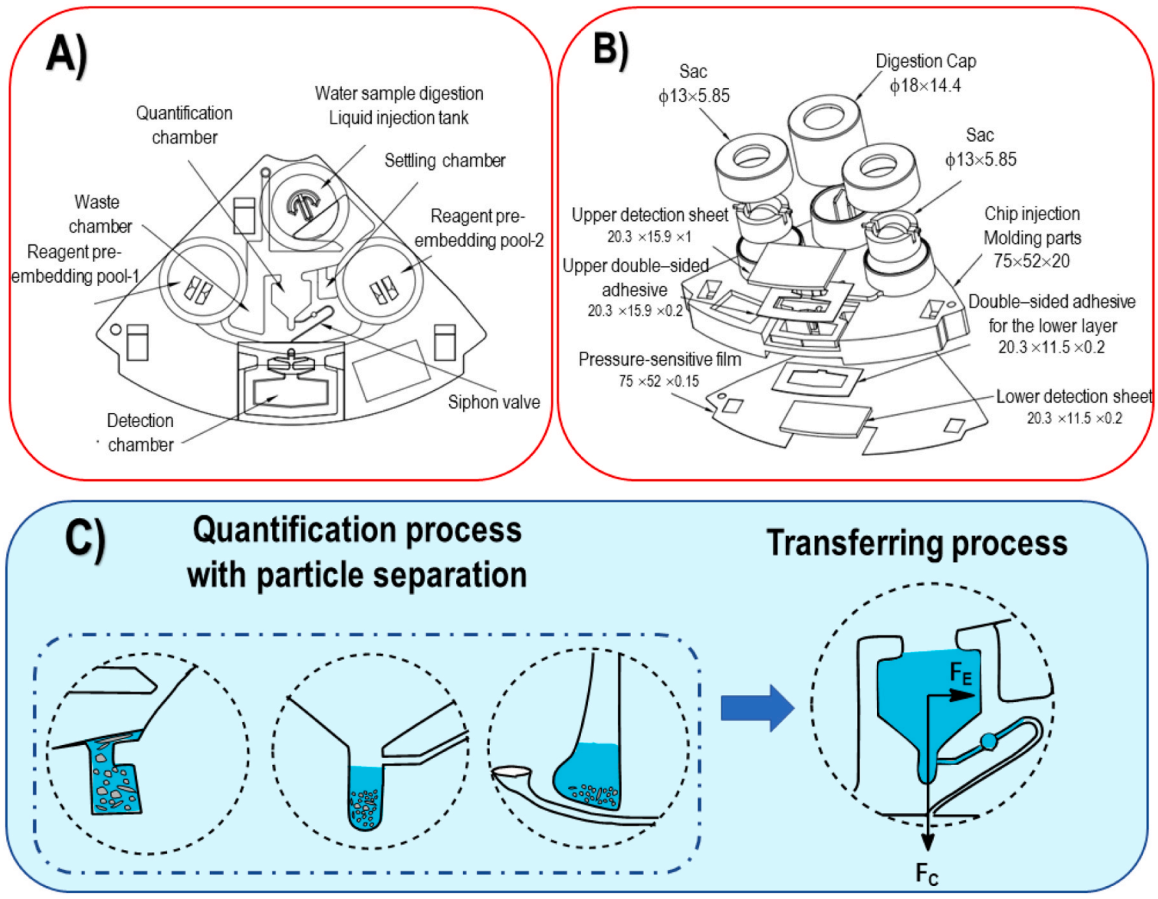

Fig. 1. Structural layout and operational process of the CMC (A) Internal schematic of the CMC showing key functional components (B) Exploded 3D view of CMC, and (C) Illustration of the chip's fluid control process: quantification of the sample in the setting chambers, followed by the transferring process.

in the detection pool, located at the bottom center of the chip. This reaction chamber serves as the primary detection zone, where absorbance measurements are performed by integrated optical sensors or external readers. The pre-embedded liquid bags (Pool ① stores redox reagent A, and Pool ② stores redox reagent B) are positioned at both ends of the fan-shaped chip contains sealed reagents (Fig. 1A). These liquid reagent bags are essential for detecting total nitrogen, total phosphorus, and ammonium, with the inclusion of additional processing steps tailored to each analyte's specific detection requirements.

PMMA offers excellent optical clarity, chemical resistance, biocompatibility, cost-effectiveness, and low weight. In our fabrication process, internal microchannels are formed by bonding an injection-molded PMMA substrate to a pressure-sensitive adhesive (PSA) film. Chip bonding is achieved by applying controlled pressure, typically between 0.2 and 0.5 MPa, for 30–120 s to ensure strong adhesion between the microfluidic component and the PSA layer (Fig. 1B). The optical transparency of both PMMA and PET supports high-quality signal detection, which is critical for accurate measurements. Unlike conventional multi-layered designs, our microfluidic chip features a simplified, layer-less PET structure that enhances CMC performance and usability by reducing fabrication complexity while preserving essential functionalities (Fig. 1B).

2.2.1.2. Microfluidic equipment design. The microfluidic equipment is a compact, field-deployable system designed for ease of use, rapid testing, and real-time data transmission. With a one-click start function and wireless connectivity, the equipment enables minimally trained personnel to perform on-site analysis and upload data to a centralized server for monitoring. Core components include digestion heating, centrifugal control, liquid injection and transfer mechanisms, a lifting module, and photoelectric detection. Weighing approximately 13 kg and measuring 250 mm × 280 mm × 315 mm in footprint, the equipment is suitable for both stationary and mobile applications (Fig. 2A.B & Figure S1 for details). Thus, the equipment features a lightweight, high-strength plastic outer shell for portability, with internal aluminum alloy structures for durability and heat management. Aerospace-grade materials and modular design enhance stability, ease of maintenance, and adaptability. Topology optimization and hollow components reduce weight without sacrificing strength. Temperature-resistant materials, shock-absorbing bases, and electromagnetic shielding ensure environmental resilience. Automated assembly and real-time monitoring support quality control and rapid diagnostics. Ergonomic controls and safety features like grounding and overload protection ensure user comfort and secure operation. Overall, it offers a robust, efficient, and user-friendly solution for on-site water quality analysis.

2.2.1.3. Microfluidic system control and operation. The code was developed in C/C++ (Figure S2). We used the STM32F407VET6 microcontroller as the central control unit for our microfluidic equipment, enabling precise regulation of rotational speed, timing sequences, and peripheral control functions (Decoding the STM32F407VET6, 2025). The detection method employed was rapid reflux digestion combined with the colorimetric technique. Electrical characterization of the motor system showed a phase angle of 25.84°, corresponding to a power factor of 0.9, indicating efficient power utilization with minimal reactive losses (Section 2S 2.4). The rated torque of the system was measured at 0.15 N·m, sufficient to maintain stable rotational dynamics under the described operating conditions. The instrument incorporates a needle-actuator assembly, driven by a stepper motor, to execute precise downward needle displacement (Fig. 2A.C & Figure S3). The system

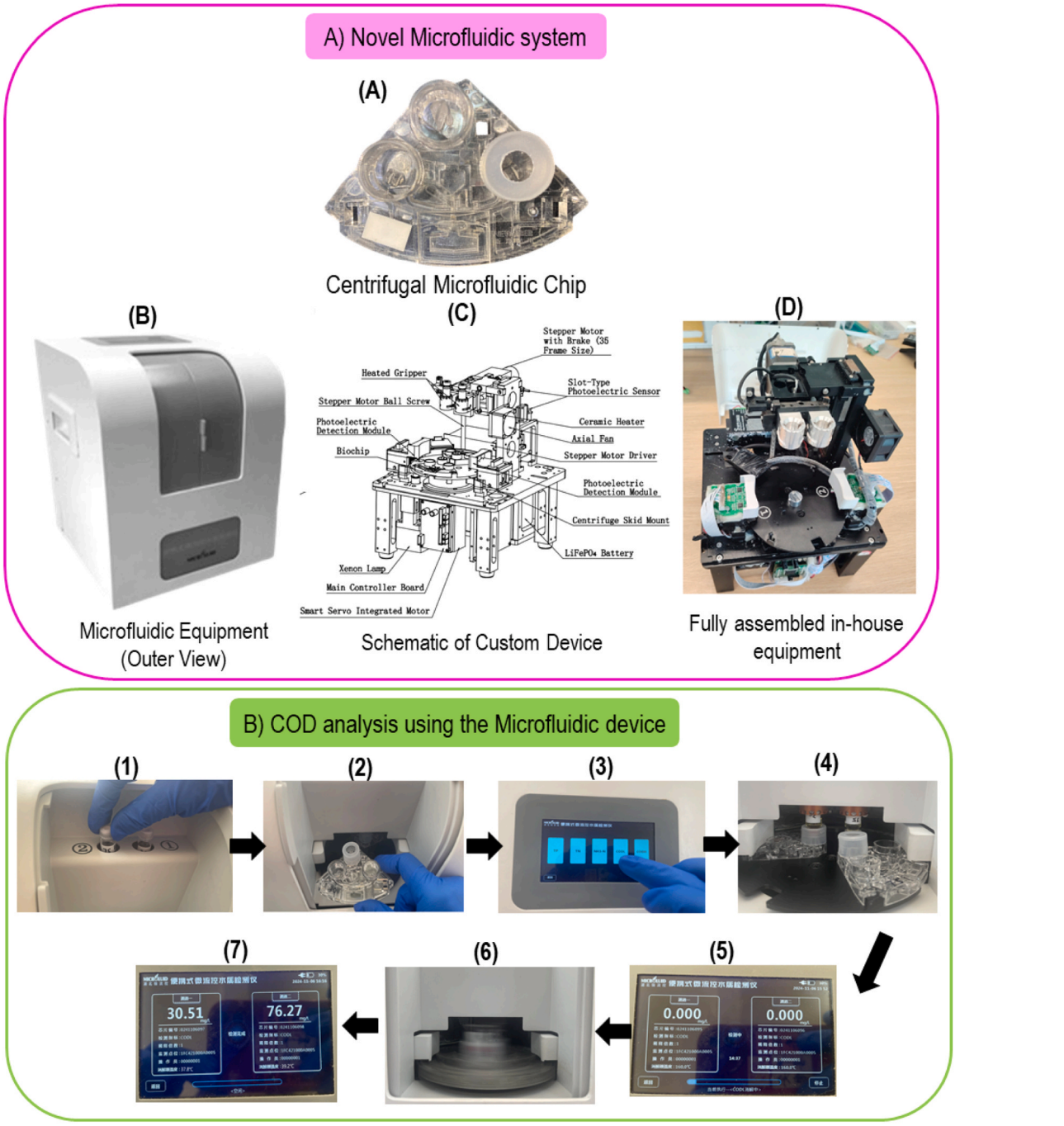

Fig. 2. A) Schematic representation of a novel centrifugal microfluidic system and associated equipment. (A) The centrifugal microfluidic chip (B). Outer view of microfluidic equipment (C) Schematic of custom design with different components, and (D) Fully assembled in-house microfluidic equipment and **B)** Step-by-step COD analysis process using the microfluidic equipment: (1) Placing the digestion valves into the instrument; (2) Introducing the microfluidic chip into the instrument; (3) Selecting the detection parameter; (4) Transferring the digested liquid into the microfluidic chip; (5) The display on the equipment shows the final temperature (165°C) when the equipment is set to measure COD; (6) Performing centrifugation; (7) The display shows the final result for COD.

comprises interconnected components centered around a logic control processor (Figure S4). The water quality detection process is carried out through a coordinated sequence of operations involving both the microfluidic chip and the automated detection equipment, each playing an essential and interdependent role (Fig. 2A.D).

2.2.1.4. Sample digestion. A digestion unit, connected via a pulse-width modulation (PWM) drive cable, is responsible for chemical digestion processes. The sample solution bottle undergoes fast digestion through a specialized heating structure (National Environmental Protection Agency, 2008) with a temperature sensor that facilitates real-time monitoring of the aqueous reagent's heating process, duration, and digestion progress (Figure S5.A). The temperature sensor's output signal is amplified by an operational amplifier, enabling the full conversion of the 0°C–165°C range into a 0V–3.3 V voltage range for enhanced accuracy (Figure S5.B). For COD measurements, conventional dichromate digestion is employed using newly developed miniaturized modules (Figure S5.C). These modules facilitate digestion at 165°C for 15 min (Fig. 2B.1). Then, the microfluidic chip was introduced into the instrument (Fig. 2B.2). Testing was then initiated via the touchscreen interface

(Fig. 2B.3). The system incorporates a component labeled "Press down to puncture," which is connected to the processor via an I/O driver. After digestion, this component rotates 180° to puncture the digestion flask and transfer the water sample to the inlet pool of the disc chip (Fig. 2B.4) (Figure S6). When set to measure COD, the equipment displays the final temperature of 165 °C on the screen (Fig. 2B.5).

2.2.1.5. Results quantification and detection. Sample quantification involves collaboration between the equipment and the chip (Figure S7). Through centrifugal rotation, the system ensures thorough filtering of large particles and mixing of the water samples with various chemical reagents, redox agents, or chromogenic agents (Fig. 1C). The quantification chamber is designed to hold 355 μL of sample, with excess flowing into the waste chamber. The entire transfer process is accomplished through the synergistic action of high-speed centrifugal force and siphon valves (Fig. 2B.6). The chip design accommodates preloaded reagents for distinct parameters.

The **photoelectric detection unit**, linked via analog-to-digital (AD) sampling, measured sample properties using optical methods. The detection pool length of this chip is 0.5 mm (Figure S8). COD measurements were carried out at 600 nm (Dhanjai et al., 2019a; Li et al., 2009). This method accurately detects characteristic frequency conversion signals, improving measurement precision and minimizing error ranges despite interference signals such as light source fluctuations and temperature drift in the photodiode (PD) (Figure S9). Optical transmission and reception offered an effective solution, enhancing detection sensitivity by reducing noise commonly observed in conventional equipment. Together, these components are managed by the logic control processor, which integrates data flow, control signals, and mechanical actions to ensure the seamless functionality of the centrifugal microfluidic equipment (Section 2S.2.4). The display presents the final result of the COD measurement clearly, allowing users to easily read and record the resulting value upon completion of the analysis (Fig. 2B.7). Further details are included in the support documentation (Section 2S).

2.2.2. Hydraulics modeling

A Computational Fluid Dynamics (CFD) module was developed to simulate CMC, enabling the identification of optimal dimensions and structural design while maximizing space efficiency within the equipment. A 2D model was created to ensure high motion accuracy and precise results, with an extremely fine mesh applied to the geometry. The motion was modeled using a rotating domain as a moving mesh, with its behavior defined globally as an interpolation function. The simulation analyzed angular accelerations versus inclination angles. All immersible fluids were computed using the Navier-Stokes equations (Eq. (1)) and the continuity equation (Eq. (2)) under laminar flow. Additionally, a time-dependent equation was used to model the system.

$$\rho\frac{\partial \mathbf{u}}{\partial t}+\rho(\mathbf{u}\bullet\nabla)\mathbf{u}=\nabla\bullet[-p\mathbf{I}+\mathbf{K}]+\mathbf{F} \tag{1}$$

$$\rho\nabla\bullet\mathbf{u}=0 \tag{2}$$

where ρ is the density of the given fluid, $\boldsymbol{t}$ is the time, $\mathbf{u}$ is the fluid velocity vector, $\boldsymbol{p}$ is the pressure, $\mathbf{I}$ is the unitary tensor, and $\mathbf{F}$ is the volume force acting on the fluid. During the numerical simulation, a no-slip condition was given for the boundary condition.

In the phase-field interface, the dynamics of two-phase flow are governed by the Cahn-Hilliard equation, which is used to track the diffusion interface, the region between two immiscible liquids, where the dimensionless phase field variable, ϕ, transitions from −1–1. The propagation of the two-phase flow interface and the initialization of the phase field are controlled by the Eq. (3):

$$\frac{\partial\phi}{\partial t}+\mathbf{u}\bullet\nabla\phi=\nabla\bullet\frac{\gamma\lambda}{\epsilon_{\mathrm{pf}}^{2}}\nabla\psi \tag{3}$$

where γ is the mobility, λ is the mixing energy density, ϵ is the interface thickness parameter, and Ψ is referred to as the phase field covariate.

Water and air as fluids, having densities of 1000 kg/m^3 and 1.61 kg/m^3 respectively, with the dynamic viscosities of 8.94×10^{-4} Pa•s and 1.86×10^{-5} Pa•s at a temperature of 20℃. The simulation, conducted using the Time-Dependent method along with Phase Initialization, couples all the physical phenomena through a Two-Phase Flow and Phase Field under the Multiphysics node.

2.2.3. Method of analysis

Both the conventional and microfluidic methods for COD detection follow the same digestion procedure, as outlined in Standard HJ/T 399–2007 (National Environmental Protection Agency, 2008). Pre-packed reagent mixtures were used, consisting of potassium dichromate ($K_2Cr_2O_7$) as the oxidizing agent, sulfuric acid (H_2SO_4) as the acid medium, silver sulfate (Ag_2SO_4) as the catalyst, and mercuric sulfate ($HgSO_4$) as the halide-masking agent. For low COD concentrations (COD $_{\mathrm{Low}}$, 0–150 mg L^{-1}), Reagent A was prepared with 0.015 mol L^{-1} $K_2Cr_2O_7$, 1.838 mol L^{-1} H_2SO_4, and 0.067 mol L^{-1} $HgSO_4$. Reagent B consisted of 5.00 g Ag_2SO_4 dissolved in 500 mL of H_2SO_4. In the microfluidic procedure, 60 μL of Reagent A and 300 μL of Reagent B were mixed with 250 μL of the sample in the digestion valve. For higher COD concentrations (COD $_{\mathrm{High}}$, 100–1000 mg L^{-1}), Reagent A was formulated with 0.15 mol L^{-1} $K_2Cr_2O_7$, 1.838 mol L^{-1} H_2SO_4, and 0.134 mol L^{-1} $HgSO_4$. In this case, 50 μL of Reagent A and 250 μL of Reagent B were combined with 350 μL of the sample in the digestion valve.

To perform COD analysis using the microfluidic method, the prepared digestion vial was placed into the instrument's designated digestion slot, and the corresponding microfluidic chip was inserted into the centrifuge disk. The test was initiated by clicking the "Start" button (Fig. 2B.3); the subsequent process was fully automated. The digestion vial was heated to 165 °C for 15 min to complete the reaction. During digestion, potassium dichromate (Cr^{6+}) is reduced to trivalent chromium (Cr^{3+}) under acidic conditions, while organic matter is oxidized to carbon dioxide (CO_2).

$$2KC_8H_5O_4+10K_2Cr_2O_7+41H_2SO_4\rightarrow16CO_2+46H_2O+10Cr_2(SO_4)_3+11K_2SO_4$$

Following digestion, the sample is introduced into the microfluidic chip, where it undergoes particle filtration. The filtered solution then flows into the chip's detection chamber for absorbance measurement. The total analysis time for the microfluidic COD method is approximately 25 min.

In the dichromate COD method, absorbance measurements at 600 nm and 440 nm are used to quantify COD levels. For high COD concentrations (100–1000 mgL^{-1}), absorbance of trivalent chromium (Cr^{3+}) at 600 nm is measured, while for low COD concentrations (0–150 mgL^{-1}), absorbance of residual hexavalent chromium (Cr^{6+}) at 440 nm is used. This approach is based on the redox behavior of chromium: at high organic loads, most Cr^{6+} is reduced to Cr^{3+}, resulting in strong Cr^{3+} absorbance and minimal remaining Cr^{6+}, making Cr^{6+} absorbance unreliable. Conversely, at low COD levels, only a small fraction of Cr^{6+} is reduced, leading to high Cr^{6+} absorbance and negligible Cr^{3+} formation, making Cr^{3+} detection unreliable. Cr^{3+} and Cr^{6+} exhibit strong visible absorbance peaks at 600 nm and 440 nm, respectively.

Chloride is the primary interference in the dichromate method, as it can be oxidized by dichromate in the presence of H_2SO_4, resulting in an overestimation of COD. To eliminate this interference, mercuric sulfate ($HgSO_4$) is added to the reaction mixture in the standard method (Quintana et al., 2018). $HgSO_4$ binds with chloride ions to form soluble mercury–chloride complexes, effectively preventing their oxidation.

$$HgSO_4+2Cl^-\rightarrow HgCl_2+SO_4^{2-}$$

A weight ratio of Cl^- to $HgSO_4$ of 1:10 should be maintained to effectively mask chloride interference (Geerdink et al., 2017). However, *the* masking efficiency of $HgSO_4$ is reliable only up to chloride

concentrations of 2000 mg L^{-1} (Carbajal-Palacios et al., 2014; Geerdink et al., 2017).

2.2.4. QA/QC and performance evaluation of COD measurements

Standard KHP solutions with concentrations of 16, 30, 75, 125, and 150 mgL^{-1} were prepared by diluting 5000 mgL^{-1} standard KHP solution, and COD was analyzed using conventional and microfluidic methods (Section 2S.3.2). Similarly, to validate the reliability of the method, certified COD solutions having concentrations of 20, 50, 75, 100, 300, 500, and 800 mgL^{-1} were analyzed using conventional and microfluidic methods. Each measurement was conducted in three replicates. The coefficient of variance (CV), accuracy, uncertainty, range, and reproducibility were calculated and compared. The detection limits and dynamic range of the two methods were also determined. The coefficient of variation is used to estimate precision. When calculating the uncertainty, the uncertainty in solution preparation and the uncertainty in absorption measurement were considered (Sanchez, 2024).

2.2.5. Analysis of real-world water samples from China and Sri Lanka

To account for the practicality of the method, environmental samples were analyzed. Water from five sewage treatment plants in China (Tangxun Lake sewage treatment plant, Sanjintan sewage treatment plant, North Lake sewage treatment plant, Huangjiahu sewage treatment plant, and Erlangmiao sewage treatment plant) and Wastewater from five industries (wastewater from a pharmaceutical factory, effluent from a sewage plant, sewage from a coal gasification plant, wastewater from a semiconductor plant and Domestic wastewater of an office park) were analyzed onsite using microfluidic instrument. Another set of 500 mL samples was collected into polyethylene bottles for conventional COD analysis. As a preservation method, sulfuric acid was added to keep the pH$<$ 2, and the samples were stored at 4 ^{0}C. Before analyzing for COD, the pH of the samples was adjusted back to 6 – 9 with 0.1 mol/L sodium hydroxide. In addition, water samples from 4 locations in Sri Lanka (Dewalagama Canal, Ma Oya, Kuda Oya, and Tap water) were collected and preserved as mentioned above and were analyzed using conventional and microfluidic methods. The Relative bias of the measurements was calculated (Dan et al., 2005) as an account of the performance of the methods. The GPS coordinates of these locations were given in Table 7.

2.2.6. Analyzing the field usability of CMC

Assessing the usability of the novel method in field applications is essential to determine its potential as a user-friendly, reliable, and efficient alternative for COD analysis, particularly in settings with limited access to resources, equipment, and power. To support this assessment, a questionnaire was developed to compare the field usability of both the microfluidic equipment and the conventional COD analysis method described in Standard Methods (5220 CHEMICAL, 2025). The questionnaire focused on nine parameters: portability, throughput, cost efficiency, multiplexity (the ability to perform multiple processes), miniaturization, ease of use, energy efficiency, programmability, and durability. These characteristics were selected because they directly influence operational performance and overall usability under field conditions. They represent the key functional attributes necessary for consistent performance in resource-constrained or environmentally challenging settings. Each question included a brief description along with a list of key performance indicators (KPIs) that respondents were asked to consider when evaluating each method. Table 2 summarizes the critical factors considered in the method evaluations.

Participants were instructed to rate each parameter on a numerical scale from 0 to 10, where 0 represented the poorest rating and 10 the highest. The questionnaire was distributed to a group of 30 individuals to ensure statistically significant results (Section 6S). The group comprised researchers, graduate students, laboratory technicians, research assistants, and engineers all of whom had prior experience with both conventional COD monitoring and the novel microfluidic equipment. The responses were collected and analyzed to compare the performance and usability of the two methods.

Table 2
Comparison of Key Performance Indicators (KPIs) for Performance of CMC microfluidic method.

No	Parameters	Key performance indicators
1	Portability	Weight, size, and ease of transport
2	Throughput	Speed of analysis and sample processing rate
3	Cost efficiency	Consumables cost and cost per test
4	Multiplexity	System design and functional compatibility
5	Miniaturization	Compactness, integration of components, and sample/reagent volume
6	Ease of use	User interface, training requirements, and automation level
7	Energy efficiency	Energy usage for one analysis
8	Programmability	Customization and automation
9	Durability	Resistance to environmental factors (dust, water, shock)

3. Results and discussion

3.1. Centrifugal microfluidic chip

The centrifugal microfluidic chip (CMC) integrates a quantification chamber, settling chamber, reagent pre-embedded pools, waste chamber, siphon valves, and detection chamber to streamline liquid handling and analysis (Fig. 1). This integration minimizes labor-intensive preparation, reducing contamination risks and enabling rapid, consistent chemical reactions while eliminating the need for external fluid control systems, thereby simplifying the workflow. In the solution release of the digestion zone, a sharp cylindrical structure punctures the silicone gasket of a headspace bottle, allowing liquid to flow into the chip by gravity (Figure S6).

The CMC operates through two distinct rotational steps: one dedicated to fluid quantification and the other to fluid transfer. These steps utilize physical forces to manipulate fluids for various processes, such as filtration and valving, as illustrated in Fig. 1C.In these systems, centrifugal force (F_C) and Euler force (F_E) are the primary drivers of fluid flow, significantly influencing radial movement (Lu et al., 2024b). Centrifugal force propels the liquid outward along the radial direction within the rotating frame, while Euler force acts perpendicular to the centrifugal force during chip acceleration or deceleration. Euler force plays a critical role in fluid dynamics, especially when changes in the platform's motion alter the forces acting on the liquid, effectively guiding its movement (Deng et al., 2014b; Li et al., 2022b). These forces, quantified by Eqs. (4) and (5), can be precisely regulated by adjusting the angular velocity (ω), as shown in Fig. 3A.

$$F_c = \rho\omega^2 r \tag{4}$$

$$F_E = \rho r \frac{d\omega}{dt} \tag{5}$$

The dual-force system efficiently transports liquid from the sample tank through the filtering and quantification chambers, along the siphon channel, and into the detection chamber. The relationship between angular velocity (ω), centrifugal force (F_C), and Euler force (F_E) during liquid release is illustrated in Fig. 1C. The Coriolis force, which acts perpendicular to fluid velocity, redirects the flow without altering its magnitude, enabling precise control within CMC (Deng et al., 2014a).

This mechanism supports fluid transfer during COD analysis through a structured four-step process, as illustrated in Fig. 3B. In CMC operation, two distinct rotational phases are employed to achieve specific functions (Fig. 3A). During the initial phase (Process I), a low angular velocity is maintained to enable effective filtering and quantification. By finely tuning the rotational speed, the resulting centrifugal force increases proportionally, ensuring accurate liquid handling. Any excess

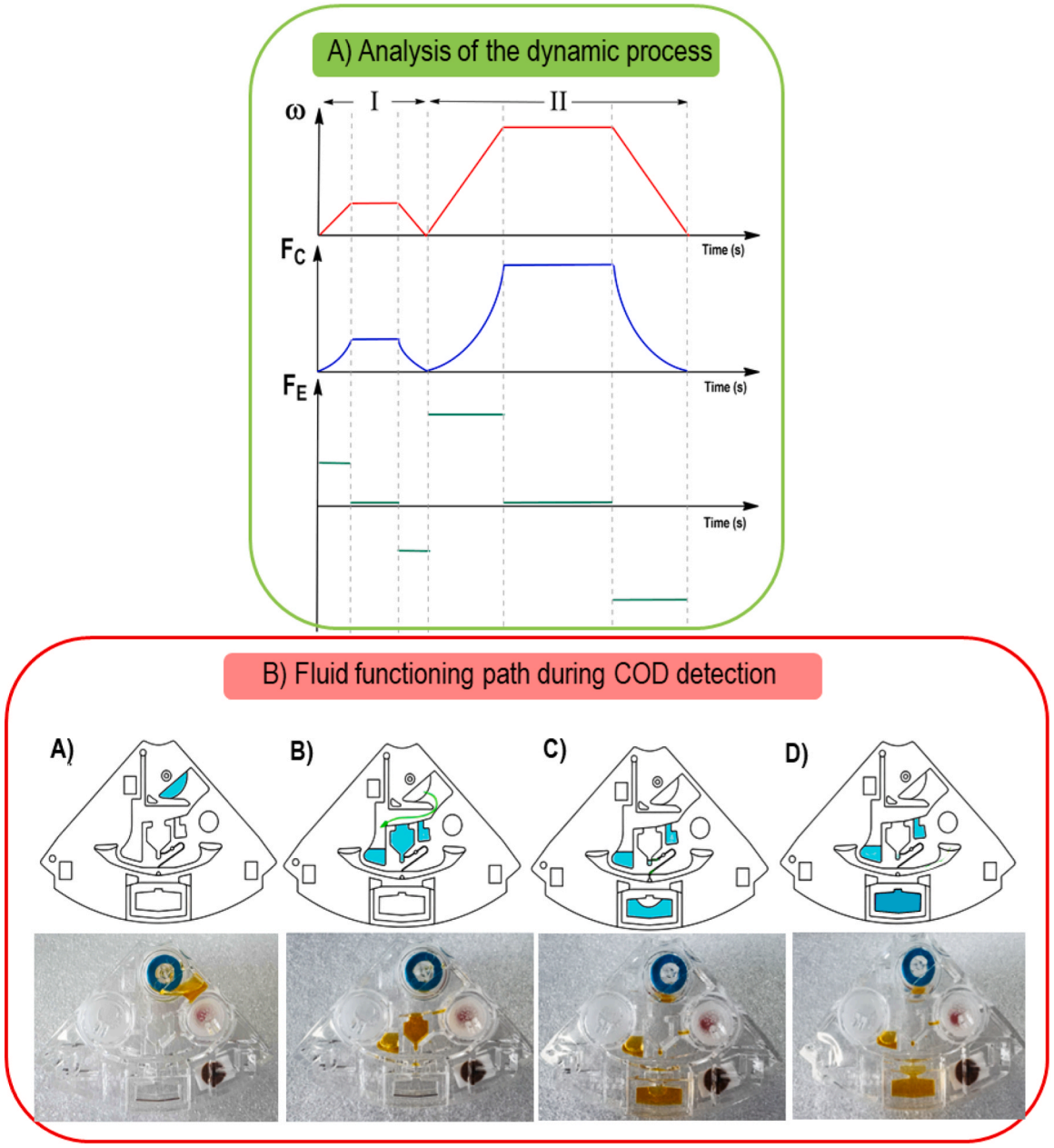

Fig. 3. A) Dynamic analysis of the system's operation, **B)** Schematic illustration, and high-speed camera images (A–D) capturing real-time fluid movement and color development on the chip during the COD detection process.

liquid is directed into a waste chamber to prevent overflow (Fig. 3B.B). In the subsequent phase (Process II), the rotational speed is further increased. This generates a sufficient driving force to overcome the siphon valve threshold, allowing controlled transfer of fluid into the detection chamber (Fig. 3B.C). During this release, the centrifugal platform also generates a transient Euler force, which surpasses the centrifugal force, efficiently propelling the sample through the connecting channel toward the detection zone (Fig. 3B.D). The schematic uses color coding to denote various reagent mixing stages; however, these colors are illustrative and do not represent final colorimetric outcomes.

Beyond COD detection, the CMC platform can be extended to measure total nitrogen, total phosphorus, and ammonium by integrating additional modules (Section 3S). Pre-filled reagent bags are embedded at both ends of the fan-shaped chip (Fig. 1A). Upon mechanical actuation, a triangular piercing element at the base of a cylindrical structure ruptures the film of each bag, releasing the reagents into designated chambers (Fig. 1A). The released liquids mix within specified zones, initiating analyte-specific chemical reactions and color development (Figure S10.D to S10.G). The system then conducts absorbance measurements to ensure precise and efficient quantification of each target compound.

3.2. Designs of geometrical parameters

3.2.1. Quantification process

By precisely controlling fluid dynamics, the quantification process ensures optimal particle separation while accurately filling the quantification chamber for seamless transfer to the detection chamber. Centrifugal force pushes larger particles outward, while smaller particles remain near the center, enabling effective separation based on size and density (Al-Faqheri et al., 2017; Lenz et al., 2021). This prevents blockages and interference with chemical reactions, minimizing light scattering or absorption in the detection pool for highly reproducible

results (Templeton and Salin, 2013a). The system maintains laminar flow, reducing turbulence and ensuring effective particle settling (AlMashrea et al., 2024). Particles are deposited in three distinct locations, minimizing cross-contamination between the sample and waste while enhancing overall efficiency. This design highlights the intricate interplay of centrifugal and Euler forces in fluid and particle control, emphasizing the need for precise geometrical and dynamic optimization for efficient microfluidic chip performance.

3.2.1.1. Setting chambers. Settling chambers are strategically integrated into the microfluidic chip to ensure accurate water sample analysis, serving as a crucial safeguard in the detection process (Fig. 1C). The system's geometry plays a key role in balancing Euler and centrifugal forces, directly impacting the efficiency of particulate matter collection. Initially, particles remain in position A due to the resultant force (Fig. 4A). Once the system reaches its target velocity, angular acceleration drops to zero ($F_E = 0$), leaving only centrifugal force ($F_C(n)$) to drive fluid movement. This force pushes fluids outward, propelling them toward the chip's edge. Pre-waste tank-1 (chamber BEFG) (4.4 × 2 × 0.6 mm) is the first filtration stage, designed to trap large particulate impurities entering through the inlet (Fig. 4A). Pre-waste tank-2 (chamber GFIH) (3.2 × 3.3 × 3 mm) collects smaller impurities, featuring a 1.7 mm diameter opening that effectively captures particles < 1.7 mm (Fig. 4A). This chamber efficiently removes impurities from aqueous samples, such as potassium persulfate suspensions in reagents. Under centrifugal force, smaller particles follow the Euler force (EF) surface and become trapped in pre-waste tank 2 (Fig. 4C, D & E). After a set period, impurities are directed into the settling chamber, such as pre-waste tank 2 (Fig. 4F). As the water sample flows along path A-B-G, it sequentially fills pre-waste tank 1 and pre-waste tank 2 before entering the quantification tank. During deceleration, as centrifugal force decreases to zero, the Euler force also diminishes, and the front waste tank fills to a height of 0.6 mm (Fig. 4G). The third filtration stage is the sedimentation collection tank (chamber JKL), measuring 1.5 × 1.3 × 4 mm (Fig. 4B). This chamber captures suspended impurities, particularly those with densities close to that of water. Fine particulate matter, less affected by centrifugal force due to its small size and density, is effectively trapped within this chamber (Templeton and Salin, 2013b), ensuring efficient separation and collection before the quantification chamber.

High-speed camera analysis reveals the intricate fluid dynamics during both acceleration and deceleration phases in centrifugal microfluidic systems. At a high angular acceleration (300 rad/s^2), the Euler force (F_E) becomes the dominant driving factor in the early phase of rotation. This results in a distinct force vector acting at an angle to the radial path, promoting early-stage impurity separation (Fig. 5A & 5B).

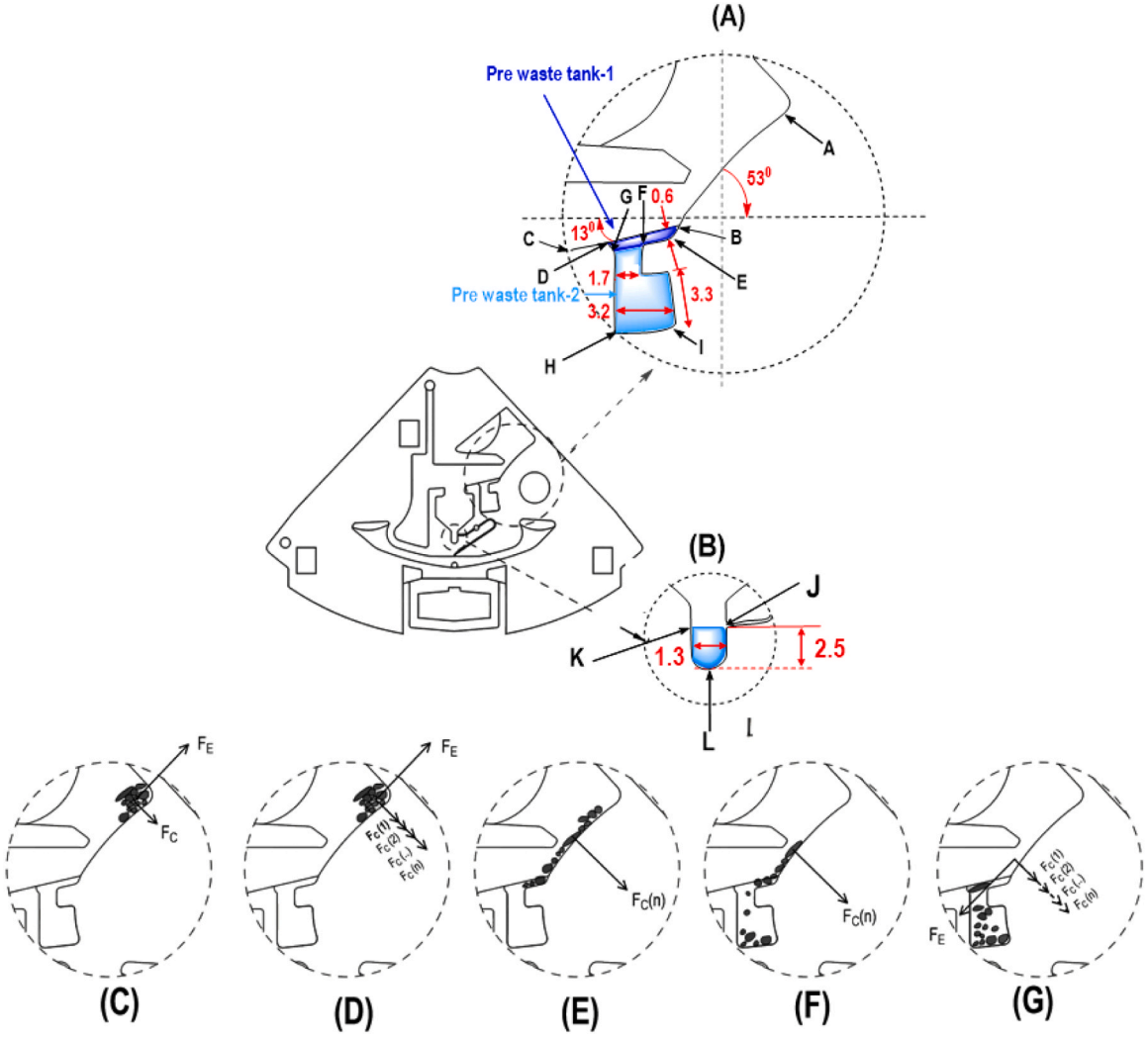

Fig. 4. Design and operation of the microfluidic chip during centrifugal particle separation. (A) Layout of pre-waste tanks 1 and 2 for sequential particle filtration. (B) Sedimentation tank (JKL) for trapping fine (C) Force dynamics during fluid flow: initial particle retention, (D–F) transition under centrifugal force, and (G) final stabilization during deceleration.

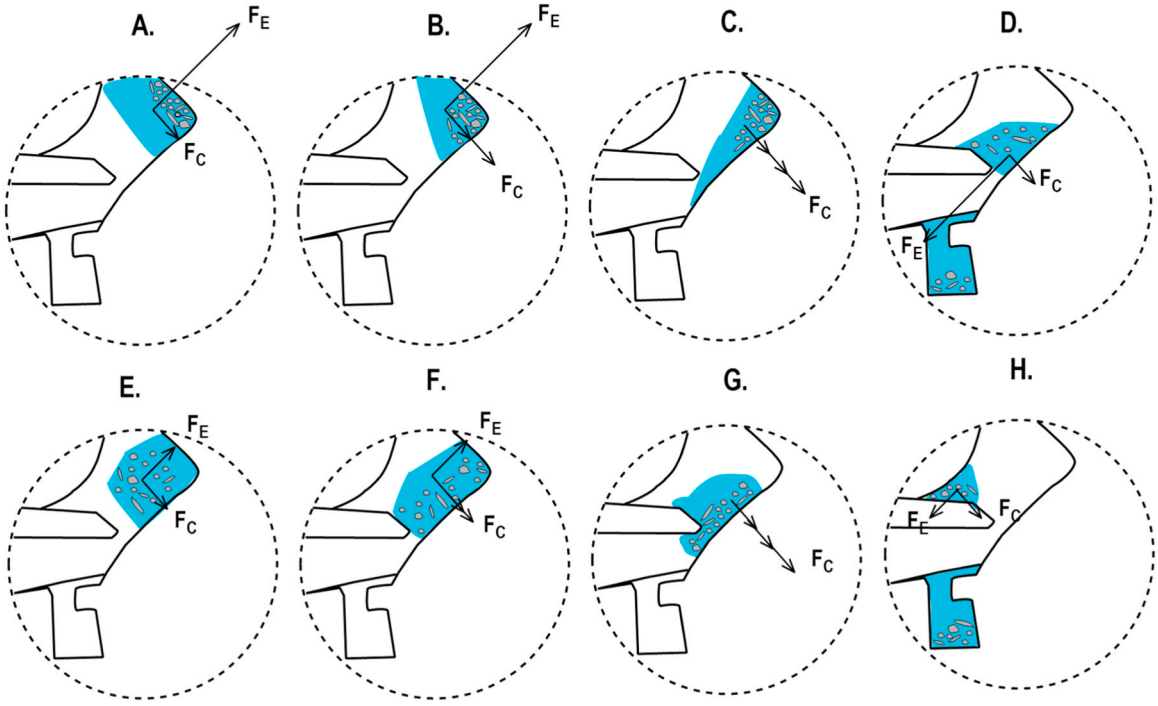

Fig. 5. Sequential stages (A–G) illustrating the behavior of fluid and particles under the influence of A-D) high angular acceleration and (E-H) low angular acceleration with centrifugal force (F_C) and Euler force (F_E) in a microfluidic chip.

However, this strong Euler force may counteract the radial fluid movement induced by centrifugal force (F_C), preventing particles and fluid from effectively reaching the pre-waste pool (Fig. 5C). During the deceleration phase, the Euler force again becomes dominant, which disrupts the intended outward fluid flow and leads to the underfilling of the quantification chamber (Fig. 5D).

In contrast, at a much lower angular acceleration (20 rad/s^2), the Euler force is minimal, but the centrifugal force alone is insufficient to propel the fluid toward the quantification zone. As a result, the liquid fails to reach the quantitative chamber altogether (Fig. 5E). Due to weak radial propulsion, the fluid remains mostly in the upper region of the pre-waste tanks (Fig. 5F&5 G). Upon deceleration, part of the fluid is redirected into the waste chamber, while solid impurities remain trapped near the injection zone, particularly in the lower edge of the injection cell (Fig. 5H).

These experimental observations demonstrate that an intermediate angular acceleration of 80 rad/s^2, combined with a target rotational speed of 750 rad/s, achieves a balance between Euler and centrifugal forces. This condition ensures efficient liquid transfer while minimizing impurity retention in undesired areas. Maintaining a constant rotation for 8 s allows precise volumetric filling of the quantification chamber. Together, these findings emphasize the necessity of carefully tailoring both the rotational profile and chip geometry to achieve reliable fluid control and effective particle separation in CMC platforms.

3.2.2. *Transferring process*

The transferring process involves the controlled movement of fluid samples through a microfluidic system, where precise management of pressure, flow rate, and fluid dynamics ensures accurate sample handling (Malloggi, 2016). Effective transferring is crucial for achieving accurate measurements, proper particle separation, and preventing backflow or unwanted mixing, thereby optimizing the overall efficiency and reliability of the system (Wang et al., 2024a). In centrifugal microfluidic platforms, centrifugal force acts radially outward, effectively replacing gravity's role in traditional siphon action to drive fluid movement. Since these chips are positioned horizontally, gravity acts perpendicular to the fluid's movement and has no impact on the siphon effect. Instead, the siphon action is entirely driven by centrifugal force, created by artificial gravity, making it independent of universal gravity (Strohmeier et al., 2015). The siphon valve controls fluid transfer by allowing flow only when specific pressure and liquid height thresholds are met, preventing backflow and ensuring smooth, precise sample movement between the quantitative chamber and detection chamber. The structural design of the siphon valve's microchannel plays a pivotal role in this process, as illustrated in Figs. 6C to 6G.

After the quantification process, the centrifugal platform generates an Euler force much greater than the centrifugal force, enabling the liquid to be released from the quantitative chamber and efficiently driven through the siphon valve into the detection chamber, as shown in Fig. 6. The movement of the liquid in the sample chamber is affected by both centrifugal and Euler forces. At lower angular velocity, the Euler force is the primary driving force (Fig. 6A). Under the influence of the Euler force, the liquid moves from the quantitative chamber, overcomes the resistance at the low crest, and flows through M_3 (Fig. 6B). As time progresses, the centrifugal force increases in magnitude and eventually becomes the primary driving force propelling the liquid radially until it fills the entire channel (Fig. 6C). When the chip reaches a constant rotational speed, the centrifugal force fully activates the liquid, transferring it from the sample chamber to the collection chamber. Once the water level in the quantitative cell drops below the M_5 point, the remaining water is continuously drawn through the siphon effect into the microchannel of the siphon valve (Fig. 6D). This process continues until the centrifugal force halts at the equilibrium pressure P_1=P_2 generated at the M_4 point. Further, it is decelerated to 0 under the action of reverse acceleration, and M_3 prevents the water sample from flowing back to the quantitative chamber (Fig. 6E). To ensure complete transfer of the water sample, it is crucial to carefully design the angular acceleration, centrifugation time, and volume of the sample in the quantitative tank. Additionally, variations in water sample density and required centrifugation times for different parameters must be considered to guarantee efficient and thorough transfer.

3.2.3. *Geometric parameters of the transfer process*

The influence of various geometric factors on the angular

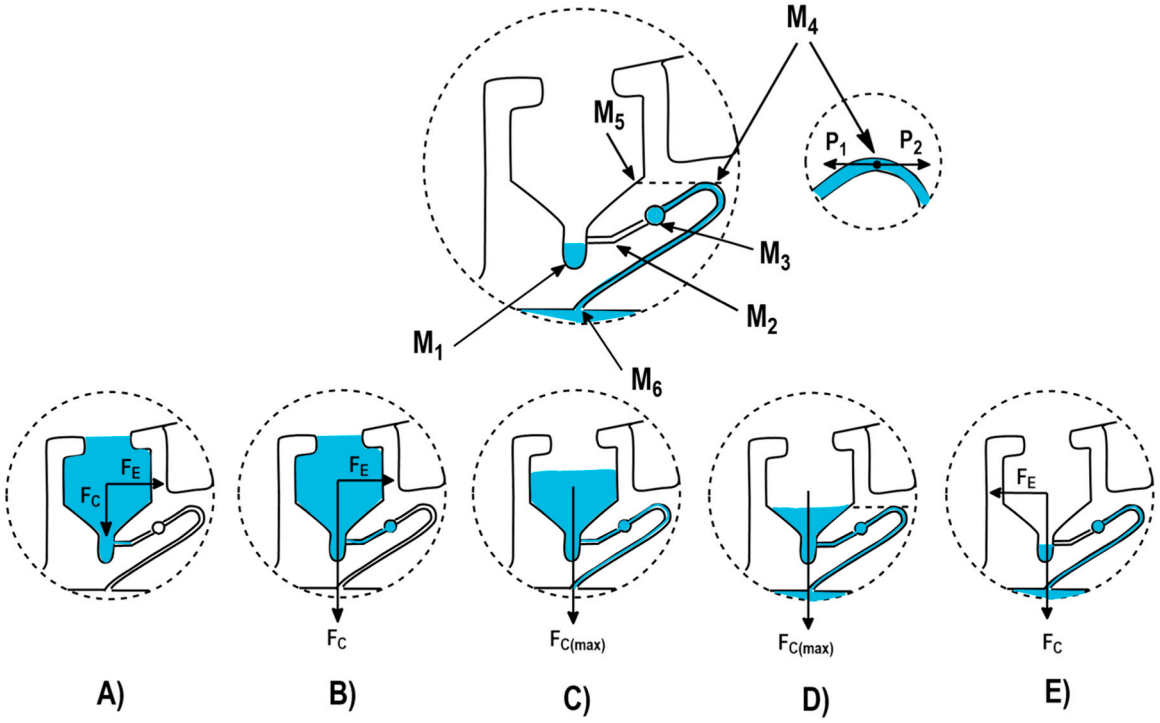

Fig. 6. Sequential liquid transfer via Euler and centrifugal forces. (A) At low speed, the Euler force (F_E) dominates and initiates inward flow. (B) F_E pushes liquid over the siphon crest (M_3). (C) Centrifugal force (F_C) reached maximum and drives flow through the siphon. (D) At steady angular velocity, the siphon continues until equilibrium at M_4 ($P_1 = P_2$). (E) During deceleration, reverse F_E prevents backflow, and M_3 blocks return flow.

acceleration is required for precise control of sequential liquid release from multiple Euler-force-driven siphon valves. The specific geometrical parameters explored with the siphon valve included the inclination angle (α), the length of the channel (l), the depth of the channel (d), the width of the channel (w), and the radius from center to siphon inlet (r) (Fig. 7A). The efficiency of the liquid transfer process heavily depends on the magnitude of the angular acceleration. To maximize the volume ratio, it is essential to define specific geometrical parameters for the microfluidic chip's siphon valve. Acting as the heartbeat of the CMCs, the siphon valve masterfully regulates fluid movement through rotational forces, ensuring precise and autonomous control that drives seamless and efficient microfluidic operations.

The selected siphon channel dimensions (0.2 mm width and 0.1 mm depth, with an aspect ratio of 0.5) are optimal for precise fluid flow control (Siegrist et al., 2010). The siphon valve is located radially, and the Euler force primarily governs its activation. As shown in Eq. (4), when the siphon valves are positioned farther from the center of rotation, their centrifugal radius increases, requiring a minimum angular acceleration for the complete release of fluid. The siphon inlet is positioned 36 mm from the center, and the disc is designed to operate within a low acceleration range of 250–750 rad/s^2. In practice, low accelerations, typically reserved for routine operations like shake-mode mixing on centrifugal microfluidic platforms, are preferred (Grumann et al., 2005). While siphon actuation at low accelerations simplifies the hardware, a negative relationship exists between the inclination angle and angular acceleration, as indicated in previous studies (Lu et al., 2024a; Li et al., 2022b).

Experiments were conducted to determine the optimal length of the siphon valve for effective liquid transfer (Section 4S). Results revealed that a siphon valve length of 19 mm or more effectively prevents leakage

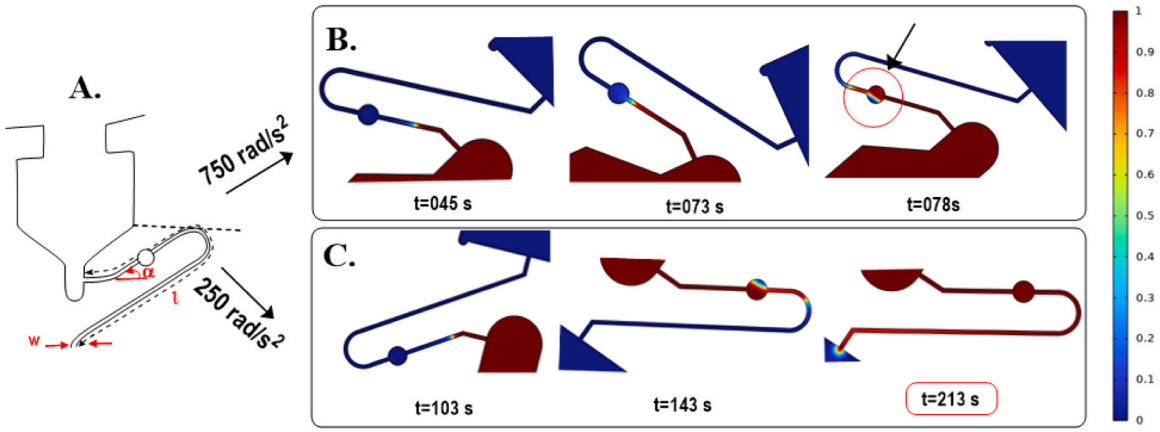

Fig. 7. (A) Schematic diagram of geometric parameters and fluid transport in a centrifugal microfluidic platform under different angular accelerations. Sequential snapshots (B) at 750 rad/s^2. and (C) at 250 rad/s^2. (Legend shows the volume fraction of fluid: blue for air, maroon for liquid, and a yellowish gradient for the air–liquid interface).

during dosing, ensuring accurate and reliable liquid transfer. At a rotational speed of 2500 rad/s, a siphon valve length of ≤ 21 mm ensures the complete transfer of samples from the quantitative chamber to the detection chamber. In time-consuming tests at 2500 rad/s, the minimum time required for the liquid to fully pass through the siphon valve was optimized at 19 mm, with a recorded duration of 45 s s. Due to the physical constraints of the chip's planar layout and limited vertical height, the maximum practical inclination angle has been experimentally determined to be 33°.

The impact of inclination angle on siphon valve operation was analyzed using CFD simulations at various inclination angles and angular accelerations. The centrifugal and Euler forces produced by the rotation of the valve structure around the axis were used to represent the volumetric force. Zero pressure boundary conditions were applied at both the inlet and outlet boundaries, while no-slip boundary conditions were enforced on all other surfaces. The contact angle of the water-wetted wall was set to 70° on PMMA (Ma et al., 2007). In the initial stage of the simulation, an extra-fine mesh was employed to construct preliminary models for identifying the optimal angle of inclination. Based on these results, an angle of 33° was selected for the second stage, as it closely matched experimental observations (Table 3). To improve accuracy, a very fine mesh was used in the second stage. The simulation was conducted in a two-dimensional (2D) domain, which inherently limits the inclusion of certain physical phenomena. A three-dimensional (3D) model incorporating all relevant physical parameters would likely provide results that more closely reflect real-world behavior.

It is important to emphasize that this simulation served as a preliminary step to validate the dimensional configuration prior to experimental trials. For enhanced precision and realism, future simulations should include additional physical effects and be performed in a fully 3D environment. At the 33° inclination, mesh refinement was applied to prevent liquid overflow, reduce abnormal pressure variations, and eliminate irregularities in the velocity vector field. The high average mesh quality indicates a lower likelihood of numerical errors, thereby enhancing the reliability of the simulation results. The numerical outcomes, presented in Figs. 7 and 8, support the validity of the selected design parameters.

As shown in Table 4, at a rotational angular acceleration of 250 rad/s^2, the liquid filling process in the siphon valve takes the longest time due to the weaker forces driving the fluid (Fig. 7 C). With lower acceleration, the liquid moves more slowly, and surface tension and viscosity effects dominate, resulting in a gradual filling process with predominantly laminar flow. In contrast, at 750 rad/s^2, the significantly higher acceleration increases the velocity of the fluid, leading to instabilities and a transition from laminar to turbulent flow (Fig. 7B).

While higher acceleration reduces filling time, 500 rad/s^2 angular acceleration with a 33° inclination angle proves to be the optimal choice for balancing efficiency and controlled flow behavior (Fig. 8). To further enhance the system, flow stabilization techniques such as modifying the siphon valve geometry or incorporating flow restrictors help minimize turbulence at higher accelerations, ensuring more efficient and precise liquid transfer.

Following siphon valve operation, the solution is fully transferred into the quantitative chamber within 50 s, reaching an angular velocity of 2500 rad/s under an acceleration of 500 rad/s^2. The subsequent sac release process is initiated by a mechanical ejector needle puncturing the capsule membrane, releasing the redox reagents A or B into the detection cell. These reagents mix with the water sample, triggering a colorimetric reaction. This integrated process guarantees precision, efficiency, and consistency in fluid handling within the microfluidic system. Efficient mixing is vital for achieving homogeneity in samples undergoing chemical reactions within the chip. Centrifugal microfluidics utilizes intrinsic forces such as the Coriolis force and external perturbations to enhance mixing. Techniques have been developed where changes in rotational speeds generate shear-driven flows that significantly reduce mixing times from several minutes to just seconds (Tang et al., 2016).

3.3. COD measurement

3.3.1. Optimization and justification of digestion time

The conventional dichromate digestion explained in the ISO method involves 2 h of reflux time (ISO, 6060, 1989; Jiang et al., 2020; Dhanjai et al., 2019b). The microfluidic method is designed to reduce digestion time, and the justification is required. A 200 mgL^{-1} COD solution was analyzed using the microfluidic method with varying digestion times. Three replicates were analyzed, and accuracy was calculated.

According to the data illustrated in Table 5, after the digestion for more than 15 min, the adsorption values of the microfluidics system are relatively stable. The digestion time of 2 h is attributed to the large volume of the samples (2 mL). In the microfluidic system, the sample volume is only 240 μL. Hence, in reduced time, it is possible to digest the organic matter in the sample and possible to give accurate COD values.

3.3.2. Method validation

The major environmental concern of the conventional COD analysis is the release of high amounts of heavy metals (Cr, Hg, and Ag) into the environment. Long reflux time and the bulkiness of the operators reduce the suitability of the method's field application (Kolb et al., 2017). The microfluidic method has reduced the volume of reagents used by 91.58 % compared to the conventional method, lowering the release of toxic chemical waste to the environment and reducing the bulkiness of the apparatus. The developed method has achieved a 55 % reduction in total analysis time, cutting the process by almost half compared to the conventional method. This directly reduces energy consumption, which is particularly advantageous for field analysis. Moreover, the microfluidic method is automated. Thus, there are no time gaps between the steps of the process. This benefit is not in the conventional method. Quick analysis is essential when analyzing rapidly changing environmental samples. Furthermore, the driving technology in the microfluidic equipment only needs an ordinary motor, which has low power consumption and requires a small space. As shown in Table 6, our method has shown an enhanced performance over conventional methods concerning accuracy & RSD (96.71 % & 2.90 %), LOQ (12 mg mgL^{-1}), sample volume (0.66 mL), analysis time (< 25 min), cost per sample, and automation capability.

3.3.3. Precision, accuracy, uncertainty, range, and reproducibility

The microfluidic method of analyzing water quality exhibits several advantages over conventional analysis. Tables 5S and 6S show standard

Table 3
Mesh elements, AEQ, and physics settings at different inclination angles and angular acceleration.

	250 rad/s^2			500 rad/s^2			750 rad/s^2		
	ME	AEQ	PS	ME	AEQ	PS	ME	AEQ	PS
63°	21,548	0.8691	Extra fine	21,548	0.8691	Extra fine	21,548	0.8691	Extra fine
53°	18,913	0.8668	Extra fine	18,913	0.8668	Extra fine	18,913	0.8668	Extra fine
43°	17,490	0.8600	Extra fine	17,490	0.8600	Extra fine	17,490	0.8600	Extra fine
33°	53,781	0.8953	Extremely fine	53,781	0.8953	Extremely fine	53,781	0.8953	Extremely fine

ME: Mesh elements, AEQ: Average element quality, PS: Predefined size.

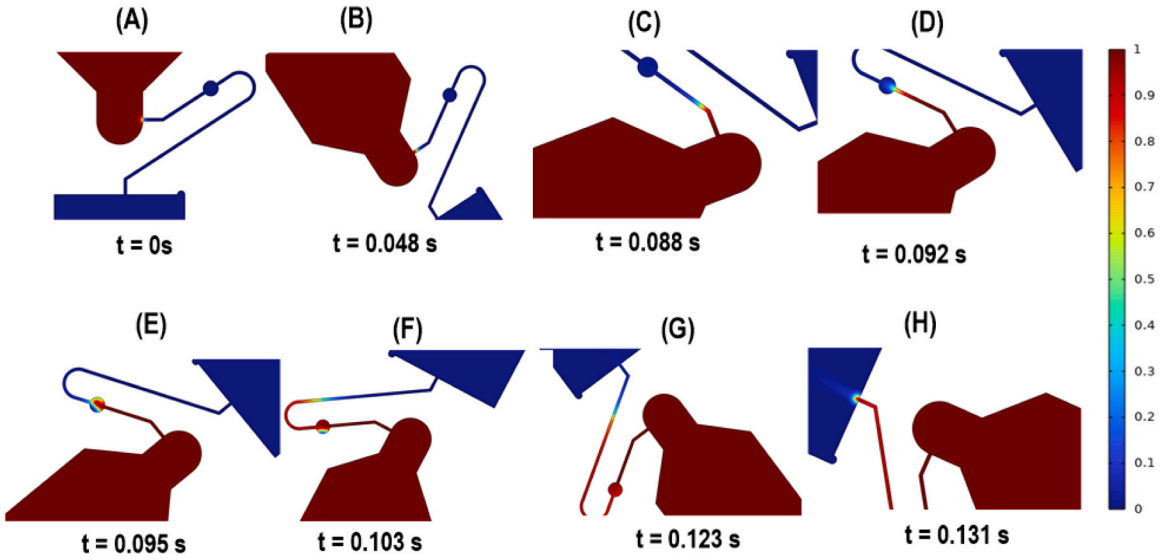

Fig. 8. Illustration of the simulation process of liquid transfer, with the gas phase depicted in red and the aqueous phase in blue. (Legend shows the volume fraction of fluid: blue for air, maroon for liquid, and a yellowish gradient for the air–liquid interface.).

Table 4
Time required for liquid filling in the siphon valve at different inclination angles and angular accelerations.

	33°	43°	53°	63°
250 rad/s^2	0.231 s	0.211 s	0.234 s	0.217 s
500 rad/s^2	0.131 s	0.134 s	0.145 s	0.142 s
750 rad/s^2	0.103 s	0.103 s	0.106 s	0.106 s

and certified sample data. Calculated data for accuracy, uncertainty, and CV is shown in Fig. 9. When standard samples were analyzed (Fig. 9A), the overall accuracy of the microfluidic method increased by 6.85 %, while the coefficient of variation (CV) used as an indicator of precision was reduced by 64.10 %. The advancement in measurement accuracy and CV is mainly due to the filtration step involved in the microfluidic chip. This process removes unwanted particulates before detection. The method of analysis is based on absorption. Hence, removing particles before analysis is important as particles cause the scattering of incident light and reduce the transmittance, which causes the reduction of the intensity of transmitted light (Templeton and Salin, 2013b) and leads to erroneous results. In addition to this, the structure of the chip is designed with air vents. As the chip operation is based on a centrifugation strategy, any air bubbles present in the sample at the detection chamber will be removed in the opposite direction of the centrifugal force and discharged outside the chip. Air bubbles also cause scattering of incident light as explained above (Figure S11). In the conventional method, removal of particles or gas does not occur, which leads to errors in COD analysis. Moreover, since the volumes are small and the system is highly controlled, there is less chance of undergoing variations. Furthermore, in our design, we use bent channels and centrifugal force drives the fluid movements. This allows for optimal mixing of reagents and results in homogenized solutions (Wang et al., 2024b; Lee et al., 2011; Kumar Thimmaraju et al., 2023). Mixing increases the CV and the reproducibility of results. The uncertainty of the novel method was improved by 47.03 %. The novel method has recorded a LOD of 4 mgL^{-1}, LOQ of 15 mgL^{-1}, and a range 0–150 mgL^{-1}. The closest reason for this is the automation of the microfluidic method, which reduces human error. Most importantly, the microfluidic method was able to improve accuracy, precision, reproducibility, and uncertainty while keeping the detection range 0–150 mgL^{-1}.

For the certified solutions of COD, the values were measured by the microfluidic method and the conventional method, and accuracy, uncertainty, and precision were calculated and compared (Fig. 9B). As the certified solution does not contain interferences such as chloride ion interference, turbidity interference, or pH interference, a small difference in accuracy, uncertainty, and CV was observed between

Table 5
Experiment designed to optimize digestion time for 100 mgL^{-1} COD solution.

Digestion time (min)	Test 1 (mgL^{-1})	Test 2 (mgL^{-1})	Test 3 (mgL^{-1})	Test4 (mgL^{-1})	Test5 (mgL^{-1})	Average (mgL^{-1})	Accuracy %
5	82.21	82.89	82.89	83.58	84.95	83.304	83.304
10	97.97	93.18	95.92	92.49	93.86	94.684	94.684
15	100.03	98.66	98.66	100.03	98.66	99.208	99.208
20	100.03	98.66	98.66	100.03	100.03	99.482	99.482
25	99.34	99.34	99.34	98.66	100.03	99.342	99.342

Table 6
Table comparing novel microfluidic method and conventional method for COD analysis. (NA: not available).

Method Name	LDR/ mgL^{-1}	LOD/ mgL^{-1}	LOQ/ mgL^{-1}	Accuracy (%) / RSD (%)	Solution volume/ mL	Analysis Time/ min	Temperature/ °C	Automation	Cost per sample/$
Current Microfluidic Method	0–150	4.00	12	96.71 2.90	0.66	< 25	165	Yes	≤ *7*
Conventional analysis	0–150	4.00	NA	90.51 8.09	6.99	< 55	165	No	≥ *28*

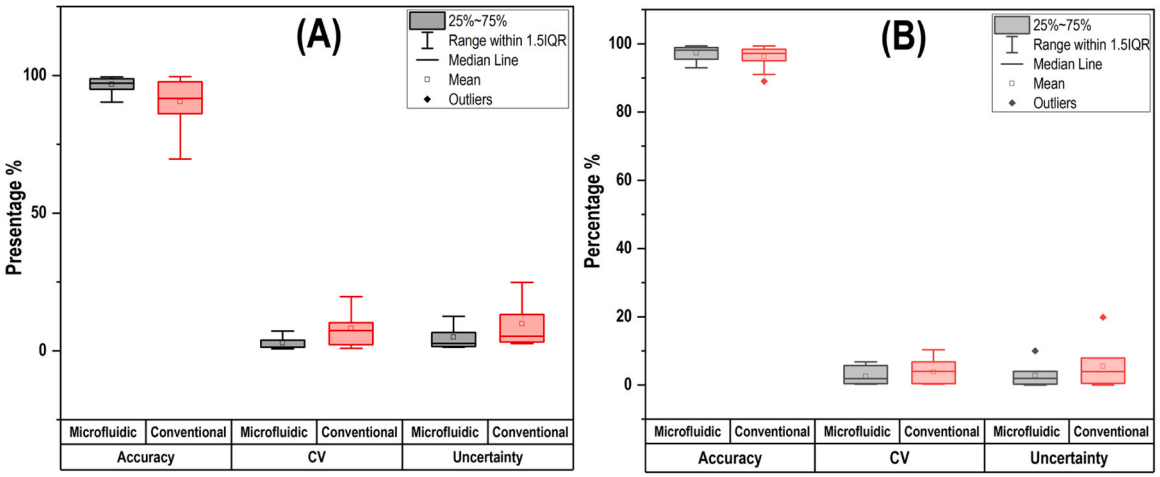

Fig. 9. Comparison the performance of the Microfluidic and the conventional method when analyzing A) standard samples and B) certified samples of COD.

measurements of microfluidic and traditional methods.

3.3.4. *Environmental samples*

Natural water samples were taken from fourteen locations, and COD values were measured using microfluidic and conventional methods. The relative bias was calculated and illustrated in Table 7. The conventional method generally yields higher COD values than the microfluidic method for most samples. This discrepancy arises because the conventional approach lacks a filtration step to remove particulate matter from the digested sample. Natural water samples often contain significant amounts of suspended particles, which remain in the cuvette during measurement. In contrast, the microfluidic instrument incorporates a filtration step that removes these particles prior to analysis. COD determination is based on light absorbance, governed by the Beer–Lambert law. A higher absorbance indicates a greater concentration of Cr^{3+}, which forms when Cr^{6+} is reduced by organic matter. Consequently, increased absorbance is interpreted as a higher COD value

3.3.5. *Validating the suitability of microfluidic and conventional methods as field instruments*

To evaluate the usability of the microfluidic equipment as a field instrument compared to the conventional method, several key performances were evaluated, including portability, throughput, cost efficiency, multiplexity, programmability, miniaturization, user-friendliness, durability, and energy efficiency. The results shown in Fig. 10 were based on the questionnaire responses of thirty participants, including researchers, graduate students, lab technicians, research assistants, and instrument developers (engineers). The results were illustrated in a spider plot (Table 7S).

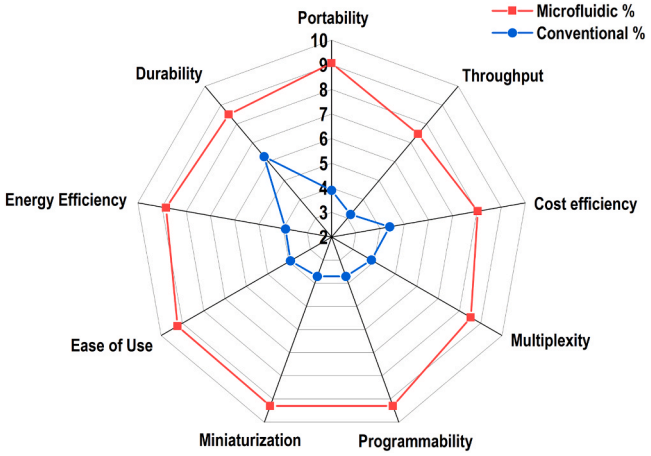

Fig. 10. Spider plot illustrating the comparative evaluation of the performance of the microfluidic device and the conventional method as a field instrument.

The microfluidic equipment received good ratings for all assessment factors, receiving ratings above 60 %. The ratings for the conventional method remained below 20 % in most cases, which indicates its limitation as a field instrument. The ratings for the microfluidic equipment increased because the equipment is small and has low reagent

Table 7
The table of performances observed for the environmental samples.

Sample	Location		Microfluidic method		Conventional method		Relative bias of (%)
	Latitude	Longitude	COD (mgL^{-1})	RSD (n = 3)	COD (mgL^{-1})	RSD (n = 3)	
Wastewater from a pharmaceutical factory	30.582211°N	114.352769°E	13202.33	2.19	13287.00	1.09	−0.64
Effluent from a sewage plant	30.235200°N	115.053360°E	42.33	3.61	43.33	3.53	−2.31
Sewage from a coal gasification plant	31.103539°N	114.350101°E	743.33	0.79	751.67	1.13	−1.11
Wastewater from a semiconductor plant	30.433933°N	114.469091°E	169.00	2.13	168.67	2.08	0.20
Domestic wastewater of an office park	30.418864°N	114.453017°E	210.33	2.39	215.33	4.21	−2.32
Tangxun Lake sewage treatment plant	30.42118°N	114.447473°E	22.67	5.09	20.00	5.00	13.33
Sanjintan sewage treatment plant	30.669722°N	114.288848°E	35.67	5.84	37.00	9.74	−3.60
North Lake sewage treatment plant	30.601300°N	114.271000°E	19.67	7.77	21.00	4.76	−6.35
Huangjiahu sewage treatment plant	30.500101°N	114.344000°E	36.33	4.20	34.00	2.94	6.86
Erlangmiao sewage treatment plant	30.587928°N	114.364275°E	42.67	4.98	31.33	4.88	−2.13
Dewalagama canal	7.285060°N	80.322238°E	14.38	7.02	12.84	4.44	−45.32
Ma Oya	7.321390°N	80.314579°E	14.96	10.12	12.19	11.51	−16.96
Kuda Oya	7.251084°N	80.331948°E	11.13	11.46	10.31	5.88	11.19
Tap Water from NIFS	7.292213°N	80.637737°E	11.36	8.55	10.39	1.36	−17.75

consumption, which improved its mobility. Moreover, the equipment is programmed and automated to take measurements and can analyze two samples simultaneously. This makes the equipment more efficient for field applications. However, the durability of the conventional method was rated at 60 %, while the microfluidic equipment received 90 %, indicating that both methods are considered durable. The conventional method received poor ratings for energy efficiency, programming ability, and multiplexity because traditional laboratory-based analysis requires manual handling and consumes high amounts of power. Altogether, the performance of the microfluidic equipment overcomes conventional methods, even as a portable device, because it shows better results than traditional approaches.

4. Conclusions

This study highlights the effectiveness of automated centrifugal microfluidic chips (CMCs) for in-situ water quality analysis, specifically in chemical oxygen demand (COD) measurement. By leveraging centrifugal and Euler forces alongside an optimized geometric design, the system enhances precision, reduces reagent consumption, and minimizes waste generation. The integration of a settling chamber further improves detection accuracy and reliability. A meticulous simulation of the siphon valve's geometrical parameters, including inclination angle and angular acceleration, led to an optimized design that ensures smooth, sequential, and stable liquid transfer into the reaction chamber, significantly reducing processing time. The microfluidic system for COD measurement enhances accuracy while significantly reducing sample volume and analysis time. With low power consumption, a compact design, and high stability, this platform offers a cost-effective, portable solution for real-time water monitoring. These advancements position CMCs as a promising alternative to conventional COD detection methods, particularly for environmental surveillance, public health, and remote water testing. Future research could explore adapting this system for detecting additional water quality parameters, further expanding its applicability across various sectors.

CRediT authorship contribution statement

CHEN X.: Writing – original draft, Supervision, Resources, Project administration, Conceptualization. **YANG W.:** Visualization, Validation, Software, Methodology, Data curation. **PAN L.:** Methodology, Formal analysis, Data curation. **B.V.N. Sewwandi:** Writing – original draft, Visualization, Data curation. **ZHANG Z.:** Formal analysis, Methodology. **Z. Wu:** Methodology, Conceptualization. **Rohan Weerasooriya:** Writing – review & editing, Supervision, Funding acquisition, Conceptualization. **A.C.A. Jayasundara:** Supervision, Formal analysis. **S.P. Hemachandra:** Validation, Methodology, Investigation. **E.G.V.P. Chandrasekara:** Formal analysis, Data curation. **K.M.N.K.B. Kuruppu:** Formal analysis, Data curation. **H.M.S.N. Deegala:** Writing – original draft, Formal analysis.

Declaration of Competing Interest

The authors declare that they have no known competing financial interests or personal relationships that could have appeared to influence the work reported in this paper.

Acknowledgements

Three reviewers' comments significantly improved the manuscript quality. The National Research Council of Sri Lanka (grant no: NRC-TO 16-015 (PPP01)) is acknowledged for its support. RW and XC thanked Distinguished Professorship at Hefei University of Technology (China).

Appendix A. Supporting information

Supplementary data associated with this article can be found in the online version at doi:10.1016/j.cherd.2025.09.019.

References

5220 Chemical Oxygen Demand (COD) - Standard Methods For the Examination of Water and Wastewater. Accessed July 22, 2025. ⟨https://www.standardmethods.org/doi/abs/10.2105/SMWW.2882.103⟩.

Al-Faqheri, W., Thio, T.H.G., Qasaimeh, M.A., Dietzel, A., Madou, M., Al-Halhouli, A., 2017. Particle/cell separation on microfluidic platforms based on centrifugation effect: a review. Microfluid Nanofluidics 21 (6), 1–23. https://doi.org/10.1007/s10404-017-1933-4.

AlMashrea, B.A., Almehdi, A.M., Damiati, S., 2024. Simple microfluidic devices for in situ detection of water contamination: a state-of-art review. Front. Bioeng. Biotechnol. 12 (February), 1–13. https://doi.org/10.3389/fbioe.2024.1355768.

Bhuiyan, W.T., Milinovic, J., Warren, B., Liu, Y. qiang, Nightingale, A.M., Niu, X., 2025. Automated Droplet-Based Microfluidic Analyzer for In Situ Monitoring of Ammonium Ions in River Water. Published online. https://doi.org/10.1021/acsestwater.4c01231.

Cai, G., Huang, Y., Chen, B., et al., 2023. Modular design of centrifugal microfluidic system and its application in nucleic acid screening. Talanta 259 (April), 124486. https://doi.org/10.1016/j.talanta.2023.124486.

Carbajal-Palacios, P., Balderas-Hernandez, P., Ibanez, J.G., Roa-Morales, G., 2014. Downscaling the chemical oxygen demand test. Environ. Technol. (U.K.) 35 (11), 1345–1349. https://doi.org/10.1080/09593330.2013.868501.

de Castro, C.M., Olivi, P., de Freitas Araújo, K.C., Barbosa Segundo, I.D., dos Santos, E.V., Martínez-Huitle, C.A., 2023. Environmental application of a cost-effective smartphone-based method for COD analysis: applicability in the electrochemical treatment of real wastewater. Sci. Total Environ. 855 (April 2022). https://doi.org/10.1016/j.scitotenv.2022.158816.

Dan, D., Sandford, R.C., Worsfold, P.J., 2005. Determination of chemical oxygen demand in fresh waters using flow injection with on-line UV-photocatalytic oxidation and spectrophotometric detection. Analyst 130 (2), 227–232. https://doi.org/10.1039/b409810b.

De Vito-Francesco, E., Farinelli, A., Yang, Q., et al., 2022. An innovative autonomous robotic system for on-site detection of heavy metal pollution plumes in surface water. Environ. Monit. Assess. 194 (2), 1–19. https://doi.org/10.1007/s10661-021-09738-z.

Decoding the STM32F407VET6 Microcontroller: From Symbol Mapping to Functions. Accessed July 19, 2025. ⟨https://www.ic-components.com/blog/decoding-the-STM32F407VET6-microcontroller-from-symbol-mapping-to-functions.jsp⟩.

Deng, Y., Fan, J., Zhou, S., et al., 2014a. Euler force actuation mechanism for siphon valving in compact disk-like microfluidic chips. Biomicrofluidics 8 (2). https://doi.org/10.1063/1.4867241.

Deng, Y., Fan, J., Zhou, S., et al., 2014b. Euler force actuation mechanism for siphon valving in compact disk-like microfluidic chips. Biomicrofluidics 8 (2), 1–18. https://doi.org/10.1063/1.4867241.

Dhanjai, Sinha, A., Zhao, H., Chen, J., Mugo, S.M., 2019a. Determination of Chemical Oxygen Demand:An Analytical Approach, 3rd ed. Elsevier Inc. https://doi.org/10.1016/B978-0-12-409547-2.14517-2

Dhanjai, Sinha, A., Zhao, H., Chen, J., Mugo, S.M., 2019b. Water analysis | determination of chemical oxygen demand. Encyclopedia of Analytical Science. Elsevier, pp. 258–270. https://doi.org/10.1016/B978-0-12-409547-2.14517-2.

Dong, Z., Zhu, X., Tang, J., et al., 2024. An integrated smartphone - based electrochemical detection system for highly sensitive and on - site detection of chemical oxygen demand by copper - cobalt bimetallic oxide - modified electrode. Microchim Acta. Published online. https://doi.org/10.1007/s00604-024-06399-w.

Farahinia, A., Zhang, W., Badea, I., 2023. Recent developments in inertial and centrifugal microfluidic systems along with the involved forces for cancer cell separation: a review. Sensors 23 (11). https://doi.org/10.3390/s23115300.

Feng, F., Ye, W.Q., Zhao, X., et al., 2025. Centrifugal microfluidic chip for multi-stage sorting and detection of microplastics at micron scale. Anal. Chim. Acta 1351 (February), 343883. https://doi.org/10.1016/j.aca.2025.343883.

Geerdink, R.B., Hurk, R.S. van den, Epema, O.J., 2017. Chemical oxygen demand: historical perspectives and future challenges. Anal. Chim. Acta 961, 1–11. https://doi.org/10.1016/j.aca.2017.01.009.

Grumann, M., Geipel, A., Riegger, L., Zengerle, R., Ducrée, J., 2005. Batch-mode mixing on centrifugal microfluidic platforms. Lab Chip 5 (5), 560–565. https://doi.org/10.1039/b418253g.

Guo, J., Brassard, D., Adam, N., et al., 2023. Automated centrifugal microfluidic system for the preparation of adaptor-ligated sequencing libraries. Lab Chip 24 (2), 182–196. https://doi.org/10.1039/d3lc00781b.

Huang, Y.H., Jiang, S., 2025. Quantification of viruses in wastewater on a centrifugal microfluidic disc. Environ. Sci. Technol. 59, 3088–3097. https://doi.org/10.1021/acs.est.4c13718.

Hwang, H., Kim, Y., Cho, J., Lee, J.Y., Choi, M.S., Cho, Y.K., 2013. Lab-on-a-disc for simultaneous determination of nutrients in water. Anal. Chem. 85 (5), 2954–2960. https://doi.org/10.1021/ac3036734.

ISO 6060. Determination of the Chemical Oxygen Demand.; 1989.

ISO15705. Water Quality — Determination of the Chemical Oxygen Demand Index (ST-COD) — Small-Scale Sealed-Tube Method.; 2002.

Jiang, H., Sun, B., Jin, Y., et al., 2020. A disposable multiplexed chip for the simultaneous quantification of key parameters in water quality monitoring. ACS Sens. 5 (10), 3013–3018. https://doi.org/10.1021/acssensors.0c00775.

Kolb, M., Bahadir, M., Teichgräber, B., 2017. Determination of chemical oxygen demand (COD) using an alternative wet chemical method free of Mercury and dichromate (Published online). Water Res. https://doi.org/10.1016/j.watres.2017.06.034.

Kumar, M., Khamis, K., Stevens, R., Hannah, D.M., Bradley, C., 2024. In-situ optical water quality monitoring sensors—applications, challenges, and future opportunities. Front Water 6 (April). https://doi.org/10.3389/frwa.2024.1380133.

Kumar Thimmaraju, M., Trivedi, R., Hemalatha, G., Thirupathy, B., Mohathasim Billah, A., 2023. Microfluidic revolution and its impact on pharmaceutical materials: a review. Mater Today Proc. Published online. https://doi.org/10.1016/j.matpr.2023.03.096.

Lee, C.Y., Chang, C.L., Wang, Y.N., Fu, L.M., 2011. Microfluidic mixing: a review. Int J. Mol. Sci. 12 (5), 3263–3287. https://doi.org/10.3390/ijms12053263.

Lenz, K.D., Jakhar, S., Chen, J.W., et al., 2021. A centrifugal microfluidic cross-flow filtration platform to separate serum from whole blood for the detection of amphiphilic biomarkers. Sci. Rep. 11 (1), 1–8. https://doi.org/10.1038/s41598-021-84353-z.

Li, J., Luo, G., He, L.J., Xu, J., Lyu, J., 2018. Analytical approaches for determining chemical oxygen demand in water bodies: a review. Crit. Rev. Anal. Chem. 48 (1), 47–65. https://doi.org/10.1080/10408347.2017.1370670.

Li, N., Shen, M., Zhu, Y., Xu, Y., 2022b. Euler force-assisted sequential liquid release on the centrifugal microfluidic platform. Sens. Actuators B Chem. 359 (February), 131642. https://doi.org/10.1016/j.snb.2022.131642.

Li, J., Tao, T., Li, X. bin, et al., 2009. A spectrophotometric method for determination of chemical oxygen demand using home-made reagents. Desalination 239 (1-3), 139–145. https://doi.org/10.1016/j.desal.2008.03.014.

Li, P., Wang, Y., Xu, B., 2022a. Research on micro-quantitative detection technology of simulated waterbody COD based on the ozone chemiluminescence method. Water (Switzerland) 14 (3). https://doi.org/10.3390/w14030328.

Lin, H., Xu, N., Xing, G., Shang, Y., Wang, X., Lin, L., 2024. Microfluidic chip-based microbial metabolism-indexed BOD sensor for rapid determination of biochemical oxygen demand. Sens. Actuators B Chem. 400 (PB), 134868. https://doi.org/10.1016/j.snb.2023.134868.

Lu, Y., Shen, H., Chen, G., et al., 2024a. Euler force-driven siphon valve control for precise sequential release in centrifugal microfluidic chips. Micromachanics 15, 1–11. https://doi.org/10.3390/mi15101200.

Lu, Y., Shen, H., Chen, G., et al., 2024b. Euler force-driven siphon valve control for precise sequential release in centrifugal micro fluidic chips. Micromachanics 15, 1–11. https://doi.org/10.3390/mi15101200.

Ma, J., 2017. Determination of chemical oxygen demand in aqueous samples with non-electrochemical methods. Trends Environ. Anal. Chem. 14, 37–43. https://doi.org/10.1016/j.teac.2017.05.002.

Ma, Y., Cao, X., Feng, X., Ma, Y., Zou, H., 2007. Fabrication of super-hydrophobic film from PMMA with intrinsic water contact angle below 90°. Polymer (Guildf) 48 (26), 7455–7460. https://doi.org/10.1016/j.polymer.2007.10.038.

Malloggi, F., 2016. Microfluidics: From Basic Principles to Applications, 917. https://doi.org/10.1007/978-3-319-24502-7_16.

National Environmental Protection Agency. Water Quality-Determination of the Chemmical Oxygen Demand -Fast Digestion Spectrophometric Method.; 2008.

O'Connell, K.C., Landers, J.P., 2023. Integrated membranes within centrifugal microfluidic devices: a review. Lab Chip 23 (14), 3130–3159. https://doi.org/10.1039/d3lc00175j.

Pol, R., Céspedes, F., Gabriel, D., Baeza, M., 2017. Microfluidic lab-on-a-chip platforms for environmental monitoring. TrAC Trends Anal. Chem. 95, 62–68. https://doi.org/10.1016/j.trac.2017.08.001.

Qu, X., Tian, M., Chen, S., Liao, B., Chen, A., 2011. Determination of chemical oxygen demand based on novel photoelectro-bifunctional electrodes. Electroanalysis 23 (5), 1267–1275. https://doi.org/10.1002/elan.201000641.

Quintana, G.O., Fagnani, E., Candello, F.P., Guimarães, J.R., 2018. The dichromate method versus the photoelectrochemical method: the synergistic influence of turbidity and chlorides on chemical oxygen demand analysis. J. Braz. Chem. Soc. 29 (3), 490–498.

Sanchez, J.M., 2024. Integrating measurement uncertainty analysis into laboratory education for the development of critical thinking and practical skills. J. Chem. Educ. 101, 4783–4789. https://doi.org/10.1021/acs.jchemed.4c00583.

Siegrist, J., Gorkin, R., Clime, L., et al., 2010. Serial siphon valving for centrifugal microfluidic platforms. Microfluid Nanofluidics 9 (1), 55–63. https://doi.org/10.1007/s10404-009-0523-5.

Strohmeier, O., Keller, M., Schwemmer, F., et al., 2015. Centrifugal microfluidic platforms: advanced unit operations and applications. Chem. Soc. Rev. 44 (17), 6187–6229. https://doi.org/10.1039/c4cs00371c.

Tang, M., Wang, G., Kong, S.K., Ho, H.P., 2016. A review of biomedical centrifugal microfluidic platforms. Micromachines 7 (2), 2–29. https://doi.org/10.3390/mi7020026.

Templeton, E.J., Salin, E.D., 2013a. A novel filtration method integrated on centrifugal microfluidic devices. Microfluid Nanofluid 17, 245–251. https://doi.org/10.1007/s10404-013-1293-7.

Templeton, E.J., Salin, E.D., 2013b. A novel filtration method integrated on centrifugal microfluidic devices. Microfluid Nanofluid. Published online. https://doi.org/10.1007/s10404-013-1293-7.

Wang, N., Dong, X., Zhou, Y., et al., 2024b. A Low-Cost handheld centrifugal microfluidic system for multiplexed visual detection based on isothermal amplification. Sensors 24 (15). https://doi.org/10.3390/s24155028.

Wang, S., Xu, Q., Cai, Y., Wang, Q., Liu, Y., Wang, D., 2024a. Biological particle separation techniques based on microfluidics. Inter. Med. 2 (2), 1–20. https://doi.org/10.1002/INMD.20240003.

Xie, S., Wu, H., Yang, X., 2024. Microfluidic electrochemical sensor for online detection of chemical oxygen demand based on AuNPs/Au electrodes. IEEE Sens. J. 24 (23), 38584–38588. https://doi.org/10.1109/JSEN.2024.3438289.

Yin, J., Zhang, Z., Zhang, X., et al., 2021. A batch microfabrication of a microfluidic electrochemical sensor for rapid chemical oxygen demand measurement. R. Soc. Chem. 2021 146, 1956–1964. https://doi.org/10.1039/d0an02133d.